NAVAL POSTGRADUATE SCHOOL
MONTEREY, CALIFORNIA

THESIS

RESISTIVITY MEASUREMENT BY EDDY CURRENT
METHODS FOR REAL-TIME MONITORING OF AGE
HARDENING IN HEAT TREATABLE ALLOYS

by

Robert Bailey James

March, 1996

Thesis Advisor: Terry R. McNelley

Approved for public release; distribution is unlimited.

19960806 012

REPORT DOCUMENTATION PAGE	Form Approved OMB No. 0704-0188

1. AGENCY USE ONLY *(Leave blank)*	2. REPORT DATE March 1996	3. REPORT TYPE AND DATES COVERED Master's Thesis

4. TITLE AND SUBTITLE: **RESISTIVITY MEASUREMENT BY EDDY CURRENT METHODS FOR REAL-TIME MONITORING OF AGE HARDENING IN HEAT TREATABLE ALLOYS**	5. FUNDING NUMBERS
6. AUTHOR(S) James, Robert Bailey	

7. PERFORMING ORGANIZATION NAME(S) AND ADDRESS(ES) Naval Postgraduate School Monterey CA 93943-5000	8. PERFORMING ORGANIZATION REPORT NUMBER

9. SPONSORING/MONITORING AGENCY NAME(S) AND ADDRESS(ES)	10. SPONSORING/MONITORING

11. SUPPLEMENTARY NOTES The views expressed in this thesis are those of the author and do not reflect the official policy or position of the Department of Defense or the U.S. Government.

12a. DISTRIBUTION/AVAILABILITY STATEMENT Approved for public release; distribution is unlimited.	12b. DISTRIBUTION CODE

13. ABSTRACT *(Maximum 200 words)*

In this research, the design of an eddy current sensor system that continuously monitors age hardening during aging of heat treatable alloys was modified to allow for operation at temperatures up to 595° C. With two eddy current coils in an impedance bridge circuit, eddy currents are generated in a pure aluminum reference sample standard and an age hardenable test sample. The difference in the resistivity of the aging test sample relative to the reference sample results in a bridge unbalance voltage, ΔV_{BCA}, which is continuously measured by a multimeter. Also, calibration procedures were developed to allow conversion of the values of ΔV_{BCA} to a resistivity difference, $\Delta \rho = \rho_{test} - \rho_{ref}$, between the test and reference samples. These calibration curves were generated by measuring ΔV_{BCA} at various temperatures for six test sample standards of known resistivity. The resistivity of the aging sample is determined by adding the known resistivity value for pure aluminum to $\Delta \rho$. Real-time monitoring of an aging alloy's resistivity may allow heat treaters to integrate this monitoring system with a control system to achieve "intelligent heat treating".

14. SUBJECT TERMS Eddy current methods, Resistivity measurement, Calibration curves, Real time monitoring, Age hardening	15. NUMBER OF PAGES
	16. PRICE CODE

17. SECURITY CLASSIFICATION OF REPORT Unclassified	18. SECURITY CLASSIFICATION OF THIS PAGE Unclassified	19. SECURITY CLASSIFICATION OF ABSTRACT Unclassified	20. LIMITATION OF ABSTRACT UL

RESISTIVITY MEASUREMENT BY EDDY CURRENT METHODS FOR REAL-TIME MONITORING OF AGE HARDENING IN HEAT TREATABLE ALLOYS

Robert Bailey James
Lieutenant, United States Navy
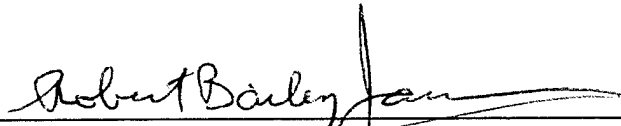B.S. Mechanical Engineering, Georgia Institute of Technology, 1984

Submitted in partial fulfillment
of the requirements for the degree of

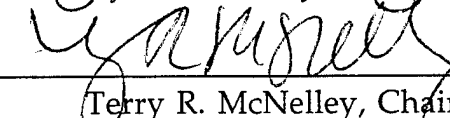## MASTER OF SCIENCE IN MECHANICAL ENGINEERING

from the

NAVAL POSTGRADUATE SCHOOL
March 1996

Author: _____
Robert Bailey James

Approved by: _____
Terry R. McNelley, Thesis Advisor

_____
Terry R. McNelley, Chairman
Department of Mechanical Engineering

iii

ABSTRACT

In this research, the design of an eddy current sensor system that continuously monitors age hardening during aging of heat treatable alloys was modified to allow for operation at temperatures up to 595° C. With two eddy current coils in an impedance bridge circuit, eddy currents are generated in a pure aluminum reference sample standard and an age hardenable test sample. The difference in the resistivity of the aging test sample relative to the reference sample results in a bridge unbalance voltage, ΔV_{BCA}, which is continuously measured by a multimeter. Also, calibration procedures were developed to allow conversion of the values of ΔV_{BCA} to a resistivity difference, $\Delta \rho = \rho_{test} - \rho_{ref}$, between the test and reference samples. These calibration curves were generated by measuring ΔV_{BCA} at various temperatures for six test sample standards of known resistivity. The resistivity of the aging sample is determined by adding the known resistivity value for pure aluminum to $\Delta \rho$. Real-time monitoring of an aging alloy's resistivity may allow heat treaters to integrate this monitoring system with a control system to achieve "intelligent heat treating".

TABLE OF CONTENTS

ACKNOWLEDGMENTS

I. INTRODUCTION

The objective of this research was to further improve an eddy current sensor system designed to continuously monitor the aging process. The sensor system was originally designed by Esarey [Ref. 1] and later modified by Mata [Ref. 2] and Hall [Ref. 3]. The improvements were to be twofold. First, the testing apparatus was to be redesigned for use at higher temperatures (such as the aging temperatures for titanium alloys). Next, a method of determining a relationship between the system output, currently in the form of a bridge unbalance voltage, and the resistivity of the test sample was to be devised. Having this relationship would allow the continuous, real-time monitoring of the precipitation hardening process.

In the precipitation or age hardening of certain alloys, the strength and hardness of the material can be increased by inducing the formation of fine and uniformly distributed precipitates in a matrix phase of the material. These fine particles act as obstacles to the movement of dislocations thereby increasing the strength and hardness of the alloy. The first step in this process is heating the alloy to a temperature within the solid single-phase region and holding. This step, called solution heat treating, dissolves any solute atoms. Next, the alloy is rapidly quenched to room temperature trapping the solute atoms and vacancies in solution forming an unstable supersaturated α-solid solution. By heating to an intermediate temperature the solutes trapped in solution precipitate, forming the desired distribution of fine particles to impede dislocation motion and increase strength. If the material remains at the intermediate temperature long enough, it will reach a point of peak strength called the T6 temper, followed by a reduction in strength due to overaging as precipitate particles coarsen .

Resistivity is a material property that is also directly affected by the aging process. Resistivity is a measure of the difficulty in passing an electric current through a metal when in the presence of an electric field [Ref. 4]. Any condition that causes free electrons to scatter will impede their net motion and increase resistivity. Events which tend to scatter free electrons and increase resistivity are: lattice vibrations due to increasing temperature; dislocations; solute atoms; precipitate particles; strain fields of precipitates;

1

vacancies; interfacial and other lattice defects [Ref. 4]. During the aging process, the resistivity of an age hardenable alloy is generally greatest immediately after quenching, when excess solute atoms and vacancies are trapped in solution and serve to cause scattering of free electrons. However, as the alloy is heated to an intermediate temperature and solute atoms are removed from solution due to the formation of precipitate particles, overall resistivity will decrease as solute atoms tend to cause more scattering events than precipitate particles [Ref. 5]. In some circumstances, the early stages of precipitation are accompanied by increased resistivity, as solutes form clusters with associated strain fields. Following this stage, the resistivity tends to decrease through the remainder of the aging process [Ref. 5]. Utilizing the eddy current sensor system already designed is one way to monitor the aging process in real time. With a proper control system, the aging process may be terminated when the desired properties of the alloy are attained.

Currently, the aging process is carried out passively according to time and temperature schedules that have been empirically shown to result in the desired mechanical, electrical, or other measured properties. Such a "cook book" approach [Ref. 3] does not take into account the variability in grain size, quench rate, or oven calibration. These and other factors affect the outcome of the aging process. Generally, the effectiveness of the aging process is not determined until the conclusion of the heat treating by destructive or non-destructive testing methods such as hardness testing or resistivity measurement at room temperature [Ref. 3]. When the results are unsatisfactory, the process must be repeated causing significant loss of time and money.

Esarey [Ref. 1], with modifications by Mata [Ref. 2] and Hall [Ref. 3], developed a monitoring system which measured the difference in inductive reactance between a test and reference coil and converted this to a voltage difference, ΔV_{BCA}, which could be monitored continuously throughout the aging process. The monitoring system contains the following components:

1) Two spiral-wound coils mounted in a ceramic testing frame;

2) A bridge carrier amplifier/filter (BCA) which includes an oscillator, impedance bridge circuit, phase sensitive demodulator, and signal amplifier/filter;

3) A Keithley 179A TRMS digital multimeter;

4) An IBM compatible PC (with a DT2801 series data acquisition board to collect time and voltage data);

5) Two K-type thermocouples;

6) Six known "flat" test sample standards (oxygen free copper (OF Cu), 99.999% pure aluminum, 1100 aluminum, T6-6061 aluminum, T6-7075 aluminum, and naval brass);

With the above equipment, ΔV_{BCA} was measured for the six test sample standards versus a pure aluminum reference sample standard at 20° C, 50° C, 75° C, and 120° C. ΔV_{BCA} was plotted against $\Delta \rho$ for the six test sample standards (although the 6061 Al and 7075 Al were not tested at 120° C due to their age hardenable characteristics) thereby generating calibration curves for resistivity for each temperature. Then, 120° C isothermal aging runs were carried out for 7075 Al to determine the viability of utilizing the system to accurately and intelligently monitor the aging process.

The following chapters will further develop the background on this subject and present redesign work on the apparatus. A more detailed description of the experimental procedures, the ΔV_{BCA} versus $\Delta \rho$ relationship, and how the problem of lift-off was dealt with will also be provided.

3

II. BACKGROUND

A. ELECTRICAL RESISTIVITY

In order to understand the operation of the eddy current sensor system, it is first necessary to discuss the origin of electrical resistivity. Electrical resistivity is the measure of the difficulty of electric current flow through a unit volume of material [Ref. 6]. Conversely, the ease of electric current passage is the electrical conductivity, the reciprocal of resistivity. In pure metals both resistivity and conductivity are temperature dependent. The unit for resistivity is the ohm-meter (Ω-m). Conductivity is often stated as a percent of the International Annealed Copper Standard (IACS), with the resistance of pure annealed copper arbitrarily assigned 100% and all other materials compared to this. Table 2.1 lists the electrical resistivity and conductivity of some common metals and alloys.

Metal or alloy	Resistivity, $\mu\Omega \cdot mm$	Conductivity, % IACS
Silver	16.3	105
Copper, annealed	17.2	100
Gold	24.4	70
Aluminum	28.2	61
Aluminum alloys		
6061-T6	41	42
7075-T6	53	32
2024-T4	52	30
Magnesium	46	37
70-30 brass	62	28
Phosphor bronzes	160	11
Monel	482	3.6
Zirconium	500	3.4
Zircaloy-2	720	2.4
Titanium	548	3.1

Table 2.1 Electrical Resistivity and Conductivity of Several Common Metals and Alloys. From Ref. [7].

A review of the table reveals that pure metals, such as silver, copper, gold and aluminum have the lowest resistivities and this is due to an abundance of free (or valence) electrons to conduct electric current as well as the relative ease of free electron motion.

In the absence of an electric field, free electron motion tends to be random and thus there is no net electron motion and, therefore, no current flow. When an electric field is applied, the free electrons move in a direction opposite to the field. In a pure crystalline solid at low temperature, wavelike free electrons can move relatively easily as they encounter few obstacles in a relatively perfect lattice. Of course, these free electrons are more likely to encounter imperfections as the crystal lattice degree of perfection decreases. These encounters, known as scattering events, serve to impede free electron motion (and thus resist the passage of electric current, as shown in Figure 2.1). Any factor promoting the scattering of free electrons will increase a material's resistivity. Such factors include lattice vibrations due to increasing temperature, dislocations, precipitates, solute atoms, vacancies, interfaces, and other lattice defects. The electron velocity in the direction of net electron motion is called the drift velocity, v_d (m/sec), and is related to the electric field, ε, by:

$$v_d = \mu_e \varepsilon \tag{2.1}$$

where μ_e is the electron mobility (m^2/V-sec). It follows that the resistivity, ρ, of a material is given by:

$$\rho \equiv \frac{1}{\mu_e n q} \tag{2.2}$$

where n is the number of free electrons in frequency and q is the charge on an electron (1.6×10^{-19} C) [Ref. 4]. In short, as scattering events become more frequent, v_d decreases and resistivity increases accordingly. It is this increase or decrease in resistivity caused by scattering events which allows the precipitation hardening process to be monitored with the eddy current sensor system.

B. FACTORS AFFECTING RESISTIVITY

From the discussion regarding scattering, it is evident that the resistivity of a metal will increase with increasing temperature, impurity content and plastic deformation. In

6

fact, the total resistivity can be represented as the sum of these components:

$$\rho_{total} = \rho_t + \rho_i + \rho_d \qquad\qquad (2.3)$$

Equation 2.3 is Matthiessen's Rule. The contributions due to temperature, impurities, and deformation are labeled as ρ_t, ρ_i, and ρ_d respectively, in Figure 2.2.
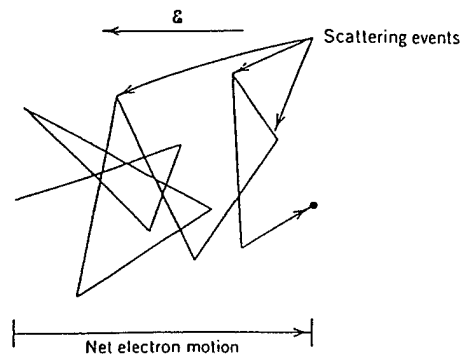
Figure 2.1 Schematic Diagram Showing the Path of an Electron that is Deflected by Scattering Events. From Ref. [4].
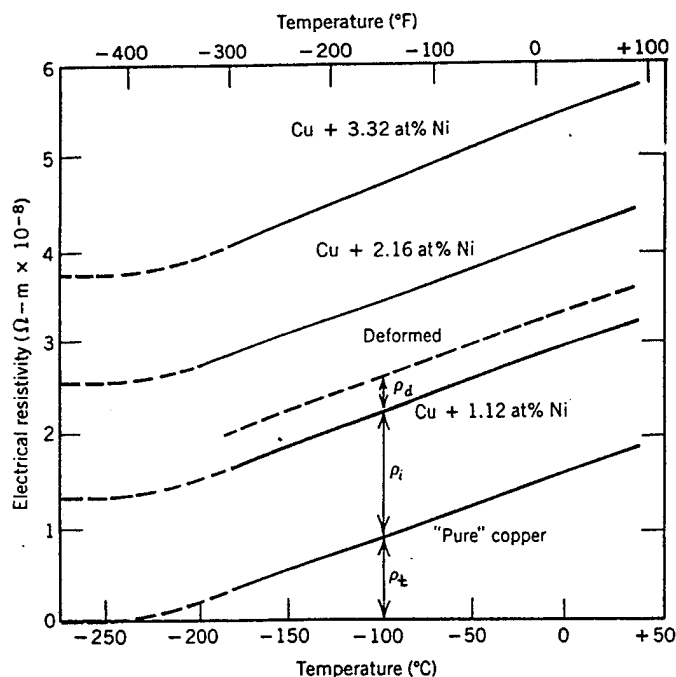
Figure 2.2 The Electrical Resistivity Versus Temperature for Copper and Three Copper-nickel Alloys, One of Which has been Deformed. Thermal, Impurity, and Deformation Contributions to Resistivity are Indicated at -100° C. From Ref. [4].

7

1. Temperature Effects

As temperature is increased, thermal vibrations in the lattice cause more scattering of free electrons, as illustrated in Figure 2.3(a-b), and resistivity increases. The resistivity at temperature, ρ_t, can be computed with the following equation [Ref. 6]:

$$\rho_t = \rho_0 + \alpha(T-T_0) \tag{2.4}$$

where ρ_0 is the resistivity at the reference temperature, T_0, and α is the temperature coefficient (Ω-m/K). As evident in Figure 2.4, the temperature coefficient is constant for a wide temperature range for Al and Cu. In fact, the temperature coefficient is constant for most metals for an appropriate range of temperatures. The resistivities and temperature coefficients of some common materials are compiled in Table 2.2.
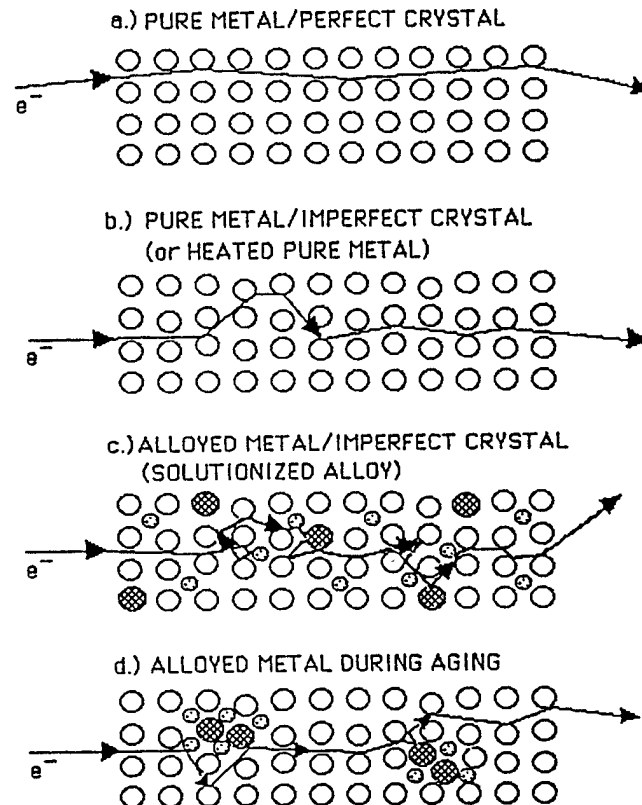
Figure 2.3 Simplified Resistivity Models. From Ref. [1].
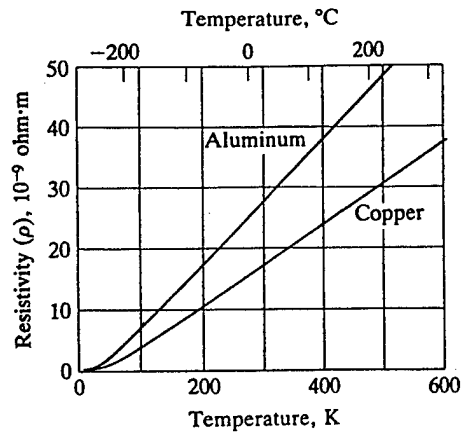
Figure 2.4 Resistivity Versus Temperature (Metals). The Resistivity of Metals is Linear with Temperature in the 100K to 500K Range (-200° C to 200° C). Except in Superconductors, the "toes" of the Curves are Finite. From Ref. [8].

	Electrical resistivity	Temperature coef.
Material	at 0°C, nΩ-m	α, nΩ-m/K
OF Cu	17.1	0.068
Pure Al	26.2	0.1145
1100 Al	29.2	0.1
6061 Al	40.0	0.1
7075 Al	52.2	0.1
Naval Brass	66.3	0.068

Table 2.2 Resistivities and Temperature Coefficients of Some Common Materials. Adapted from Ref. [9].

2. Effects of Impurities

The effect of impurities, e.g., interstitial and substitutional impurity atoms or point defects like vacancies, is to increase resistivity. The addition of such impurities increases the number of scattering events and decreases the mean free paths and time between collisions as seen in Figure 2.3 (c). The resistivity increase due to adding small amounts of other elements to copper at room temperature is illustrated in Figure 2.5.

3. Effects of Plastic Deformation

Plastic deformation increases electrical resistivity, as seen in Figure 2.2, by increasing the number of scattering events. Free electrons are scattered due to the elastic

9

strain field associated with the distorted lattice surrounding a dislocation [Ref. 10]. In this work, any materials that were cold worked were then subjected to full or stress-relief annealing prior to testing in the eddy current sensor system in order to eliminate the effect of plastic deformation. The effect of dislocations on resistivity due to decreases with both time and temperature as they take up positions of minimum energy [Ref. 11] and diminish in number due to absorption into dislocation sinks or by mutual annihilation [Ref. 3].
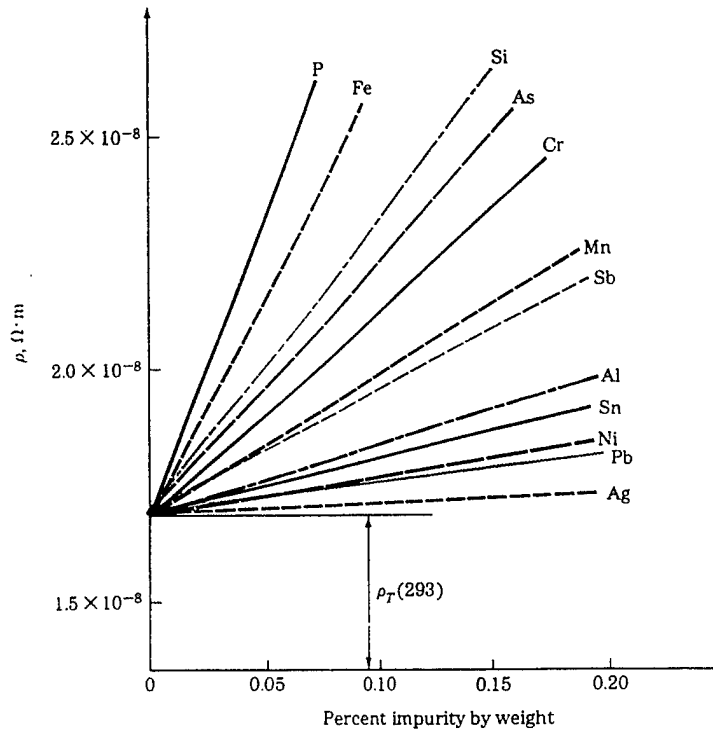
Figure 2.5 The Effect of Small Additions of Various Elements on the Room Temperature Electrical Resistivity of Copper. From Ref. [6].

4. Effects of Precipitation (Aging)

For age hardenable alloys, the total resistivity is not constant during an elevated temperature hold for an extended period of time. Instead, the resistivity is a combination of both temperature and time effects:

$$\rho_{total}(T,t) = \rho_t(T) + \rho_i(t) \tag{2.5}$$

10

where T is temperature and t is time. Such alloys can be solution treated and quenched, trapping excess solute atoms and vacancies in solution. Upon subsequent heat treatment at an intermediate temperature, the excess solutes begin to precipitate from solution. As the solutes diffuse and form clusters, called Guinier-Preston Zones (G.P. Zones) [Ref. 4], their associated strain field will cause free electrons to scatter and initially resistivity will increase. As diffusion continues, the G.P. Zones increase in size and form precipitate particles. Now, as more precipitates form and grow, the excess solutes are removed from solution providing a more unobstructed electron path and resistivity decreases. Figure 2.3 (c-d) shows how removing the solute atoms from solution has reduced the number of scattering events and increased the mean free path causing resistivity to decrease. With the eddy current system we will be able to monitor, in real time, the change in resistivity due to the aging process alone.

C. EDDY CURRENT INSPECTION

1. Eddy Current Theory

Eddy current inspection is a non-destructive form of testing based on the principles of electromagnetic induction [Ref. 7]. It is used to identify cracks, voids and other defects. It is also used to measure the resistivity of metals, which is the focus of the work in this paper. By using eddy current inspection techniques to measure a metal's resistivity, we can continually monitor the aging process in heat treatable alloys. Additional uses and techniques of eddy current inspection are detailed in References 5, 7 and 12-14.

Placing a sample to be monitored adjacent to an electric coil in which an alternating current is flowing induces eddy currents to flow in the sample. In Figure 2.6, the eddy currents flowing in the flat sample were generated by the exciting current in the coil. The induced eddy currents oppose the current flowing in the coil, thereby increasing the impedance of the coil. If resistivity decreases, these induced eddy currents will increase providing more opposition to current flow in the coil and the probe coil impedance will increase. The magnitude of these eddy currents depends on the magnitude and frequency of the alternating current in the coil, and the magnetic permeability and resistivity of the sample. In this work, the current frequency is a constant 52 kHz and all

samples have a magnetic permeability of 1.0, so the only factor affecting the magnitude of the induced eddy currents (and thus affecting the impedance in the coil) is the resistivity of the sample.
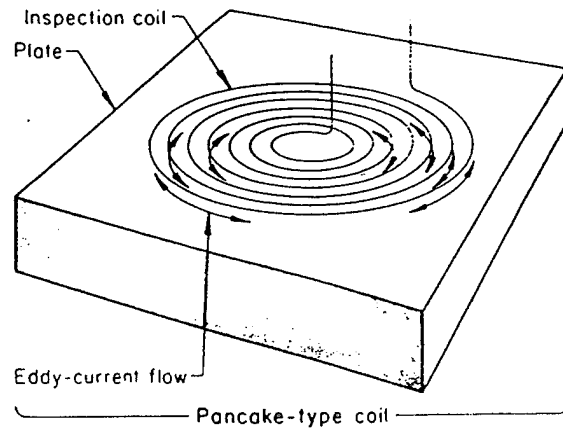
Figure 2.6 Pancake-type Coil Showing the Patterns of Eddy Current Flow Generated by the Exciting Current in the Coils. After Ref. [7].

Using a coil arrangement similar to Figure 2.7, a 99.999% pure Al sample was placed over the reference coil and a test sample over the second coil. Each coil monitors the change in resistivity of their respective sample. If the system was at a high enough
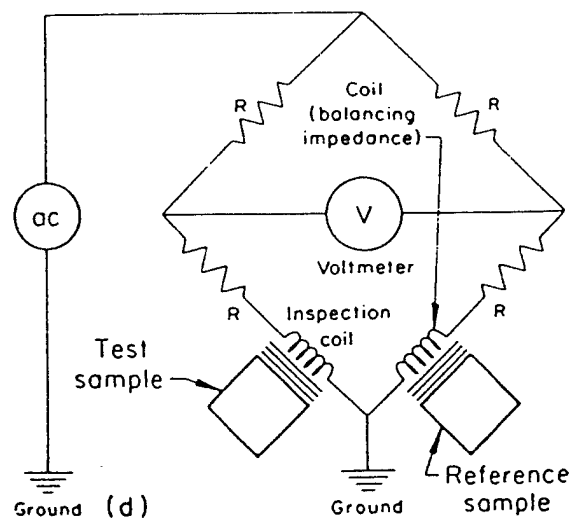
Figure 2.7 Impedance Bridge with Dual Coils and a Reference Sample in the Second Coil. After Ref. [7].

12

temperature and the test sample was a precipitation hardenable alloy, then the test sample coil impedance would increase as the test sample resistivity decreased. At the same time the reference sample (pure Al) resistivity would remain constant as would the reference coil impedance. The difference between the two impedances creates a bridge unbalance voltage which can be measured with a voltmeter. By finding the relationship between this voltage and the resistivity of the test sample, we will be able to continually monitor and gage the effectiveness of the heat treatment process.

2. Other Factors Affecting Eddy Current Measurements

a. Edge Effect

Edge effect is the distortion of the eddy currents as the inspection coil nears the edge of a sample being inspected. In general, it is advisable not to let the inspection coil come within 0.32 cm (0.125 inch) of the test sample edge [Ref. 7].

b. Skin Effect

The phenomenon known as skin effect refers to the fact that eddy currents are most dense at the sample surface in contact with the coil and become less dense as the distance from the surface increases, eventually becoming negligible. The standard depth of penetration is the depth where density is reduced to about 37% of the density at the surface. The standard depth, S, can be computed from the following equation:

$$S = 1980\sqrt{\frac{\rho}{\mu f}} \tag{2.6}$$

where ρ is the resistivity (Ω-cm), μ is the magnetic permeability (1.0 for non-magnetic materials), f is the inspection frequency (Hz) and S is in inches. From Equation 2.6 we see that S increases with increasing ρ and decreasing μ or f. A sample with a thickness of two to three times the standard depth should experience no significant size effects on eddy current measurements [Ref. 7].

13

c. Lift-Off Factor

Small variations in the spacing between the surface of the coil and the part being inspected can have severe effects on the coil impedance. Such variations in spacing are called "lift-off" [Ref. 7]. Any condition other than having the sample rest completely flat on the inspection coil reduces the eddy currents flowing in the test sample. This provides less opposition to current flow in the inspection coil and results in a lower test sample coil impedance. This results in a higher output voltage in the test set-up used in this work. Great care must be taken to ensure that lift-off is eliminated in any samples used or to devise a method of developing a lift-off correction (LOC) to eliminate unwanted lift-off contributions to resistivity measurements.

D. PRECIPITATION HARDENING

1. Background

The objective of precipitation hardening in a binary alloy is to create a uniform dispersion of fine particles on slip planes. These precipitate particles act as barriers to the movement of dislocations which can give the precipitation hardened alloy its high strength.

a. Characteristics of Precipitation Hardenable Alloys

The basic feature of precipitation hardening is that when the solute concentration in an alloy exceeds the limits of solubility for the matrix, then second-phase particles will nucleate and grow to satisfy equilibrium conditions [Ref. 10]. For this we must have an alloy system with a solvus line indicating solid solubility decrease with decreasing temperature. Figure 2.8 shows a typical phase diagram of a binary alloy which meets such criteria. The solid solubility in the α phase decreases from point a to b and temperature decreases from T_1 to T_3.

b. Procedure

Precipitation hardening is a three-step process. First, the alloy is heated to a point between the solvus and solidus lines (point c in Figure 2.8) and held there until a uniform solid solution of the α phase is produced. This step is known as solutionizing. In the second step, quenching, rapid cooling of the sample (usually to room temperature)

14
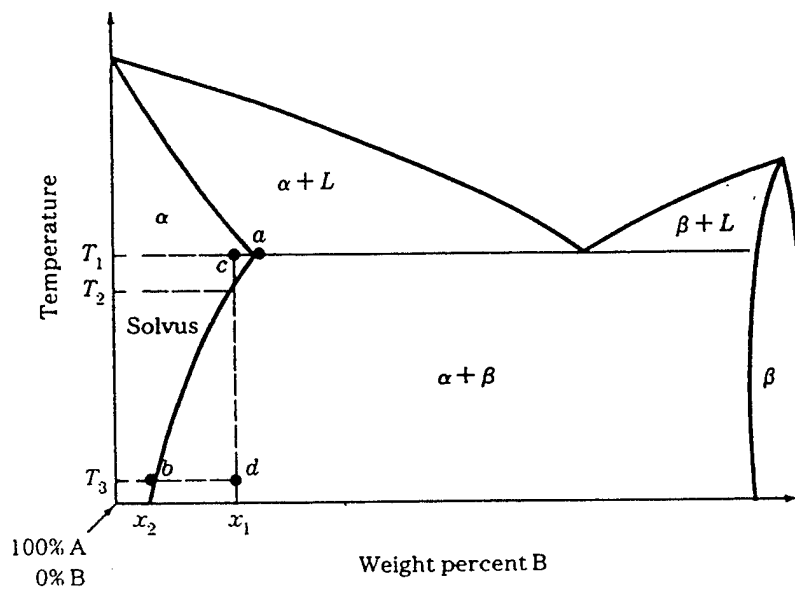
Figure 2.8 Binary Phase Diagram for Two Metals A and B Having a Terminal Solid
Solution α which has a Decreasing Solid Solubility of B in A with Decreasing
Temperature. From Ref. [6].

results in formation of a supersaturated solid solution of α phase. In Figure 2.8 the alloy

x_1 was cooled to temperature T_3. Finally, the alloy is subjected to aging. During artificial

aging, the alloy is reheated to an intermediate temperature below the solvus, usually 15 to

25 percent of the solutionizing temperature [Ref. 10]. The second heating is required to

promote the nucleation and growth of second-phase precipitation particles (β phase in the

alloy x_1). When an alloy is aged at room temperature, it is called natural aging. Aging

produces the desired fine, uniformly dispersed precipitates that increase strength. For our

work, 7075 Al was chosen and was solutionized at 480° C for 50 minutes, quenched, and

artificially aged at 120°C for various time periods from one to 24 hours [Ref. 15].

2. Effect on Hardness

The aging process is well represented by Figure 2.9 as a plot of strength or

hardness versus time (known as an aging curve). The strength is lowest immediately after

quenching, increases to a peak value, and then decreases if there is sufficient time at

temperature. At the start of the aging process, the supersaturated solid solution is highly

unstable. The alloy tends to seek a lower free-energy state which is the driving force for

precipitation. The G.P. Zones will form first. These clusters of solute atoms (regions with

high concentrations of B atoms for alloy x_1) form in a matrix of mostly A atoms. As the

15
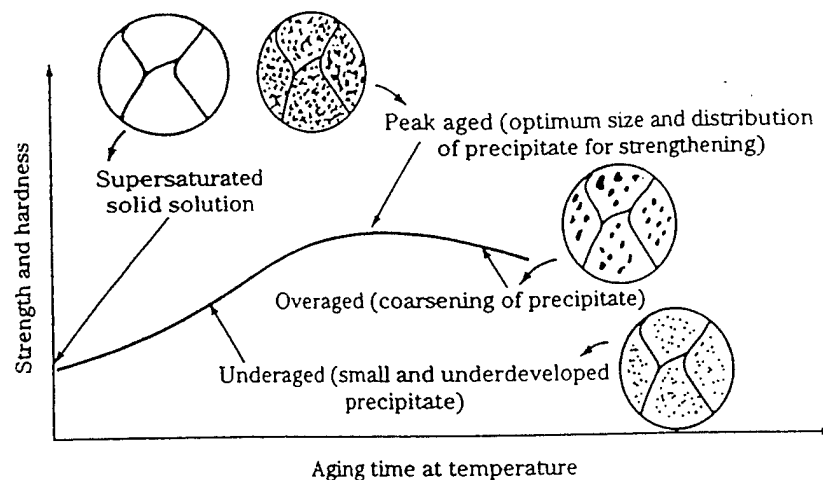
Figure 2.9 Schematic Aging Curve (Strength or Hardness vs. Time) at a Particular Temperature for a Precipitation-hardenable Alloy. From Ref. [6].

alloy remains at elevated temperature, these clusters grow into metastable precipitates. As these precipitates continue to nucleate and grow, the alloy approaches a level of peak strength known as the T6 temper. This level is listed as "peak aged" in Figure 2.9. However, if the alloy remains at elevated temperature beyond this point, the precipitates begin to coalesce and coarsen, seeking to reduce surface area and lower their total free-energy. When this happens, the strength is lowered as well, since the dislocations can now easily bend around the precipitates as they are further apart. This circumstance is known as "overaging". The key to successful precipitation hardening is to remove a given sample from the elevated temperature at the precise moment that peak aging is attained. The only way to ensure this occurs is to develop a system that monitors strength or hardness in "real time". In this work, the eddy current monitoring system measures ΔV_{BCA}, which is directly related to the resistivity of the aging sample. Since resistivity is directly related to hardness, we have a means of monitoring the aging process in real time.

3. Effect on Resistivity

With the exception of a slight initial increase in resistivity due to G.P. Zone formation (as discussed previously), the resistivity continually decreases throughout the aging process. As solutes are removed from solution, free electrons are provided with an

increasingly unobstructed path, and resistivity decreases accordingly. This continues through peak aging. The peak aged resistivities of known alloys is well documented. By continuously monitoring resistivity we can "intelligently" terminate the aging process when the resistivity reaches the value corresponding to peak aged condition rather than rely on the "cook book" time.

Currently, resistivity measurement at room temperature is a primary means of determining if the heat treating process was successful. By measuring this property during real-time monitoring, we can not only determine the success of the heat treating process, rather we can ensure success.

E. INTELLIGENT PROCESSING

The economic success of most processes depend to a large extent on how well they are controlled [Ref. 16]. It is time to couple the concept of real-time monitoring with modern control systems in order to "intelligently" heat treat precipitation hardenable alloys. In this manner, heat treaters can actively play a role in ensuring the success of each aging run rather than wait passively and let a myriad of variables determine the fate of parts being heat treated. This work explores a real-time monitoring system utilizing eddy current methods which may provide the basis for an intelligent processing system that can help ensure success in heat treating.

18

III. APPARATUS DESIGN AND REDESIGN

A. NEW REQUIREMENTS OF APPARATUS

1. Temperature

The first version of this apparatus was fabricated primarily of an aluminum alloy, except for the Teflon coil support bar and bobbins. Due to the use of the Teflon material, the maximum working temperature for the apparatus was approximately 180° C. It was desired to increase the working temperature of the apparatus to accommodate the aging temperature of titanium α-β alloys. This requirement would necessitate operation at temperatures from 480-595° C [Ref. 15]. For this purpose, the apparatus framework, probe support bar, coil bobbins and wire had to be redesigned and replaced.

2. Test Sample Geometry

The initial test samples had a geometry that was compatible with a tensile testing machine. The test sample dimensions were 20.32 cm (8.0 in) length x 2.54 cm (1.0 in) width x 0.32 cm (0.125 in) thickness. Previous work had indicated that these samples tended to distort upon quenching from solutionizing temperature to room temperature, leading to a variation in the extent of lift-off [Ref. 3]. Lift-off will be discussed in later sections of this work. Therefore the new apparatus would have to accept the current test sample geometry as well as thicker, shorter samples less susceptible to distortion and lift-off effects.

B. COMPONENT REDESIGN

With the new requirements established, the task of redesigning the initial apparatus to meet these needs proceeded.

1. Apparatus Framework

Since the previous apparatus performed well in hundreds of test runs, and in the interest of expediting the design and manufacturing process, the basic design was retained but with several important changes. The entire framework was designed to be machined from a ceramic material that could sustain the 480-595° C working temperature.

Previous research by Mata [Ref. 2] had been done and ceramic stock was purchased, which could be utilized in making the new apparatus. The ceramic material obtained was "MAKOR® Machinable Glass Ceramic by DuPont". Its continuous operating temperature of 800° C exceeds the 595° C maximum working temperature and the machining tolerances were surprisingly tight, (± 0.0005"). In addition, its coefficient of thermal expansion matches that of stainless steel so that mechanical fasteners could be bought "off the shelf" rather than machined from MAKOR stock.

Additional MAKOR materials were purchased, parts were machined, and the apparatus was assembled. The apparatus consists of four side supports attached to a baseplate, a centering guide, one end bar, one probe support bar, a thermocouple connection mechanism, two probe coils, and numerous spacers. Figure 3.1 shows the top and side views of the assembled apparatus (minus the thermocouple mechanism). As seen in Figure 3.1, the probe support and end bars can be raised or lowered to accept any sample thickness. Lengths greater than or equal to six inches can be accommodated by the configuration shown in Figure 3.1 or the apparatus can be reconfigured to accept lengths as short as three inches. Finally, the width can be reduced from the 1.0 inch nominal dimension by the use of 0.125 inch spacers.

2. Thermocouple Connection

In previous work by Hall [Ref. 3], two K-type thermocouples were connected to the apparatus with a lever and spring device in order to accurately measure the temperature of the reference and test samples. Preliminary research indicated that the manufacturing of a spring capable of operating at the design temperature was economically unfeasible. A much simpler weighted lever was designed to provide the connection between the thermocouple leads and the reference and test samples. The mechanism was not only cost effective but performed without incident in hundreds of test runs.
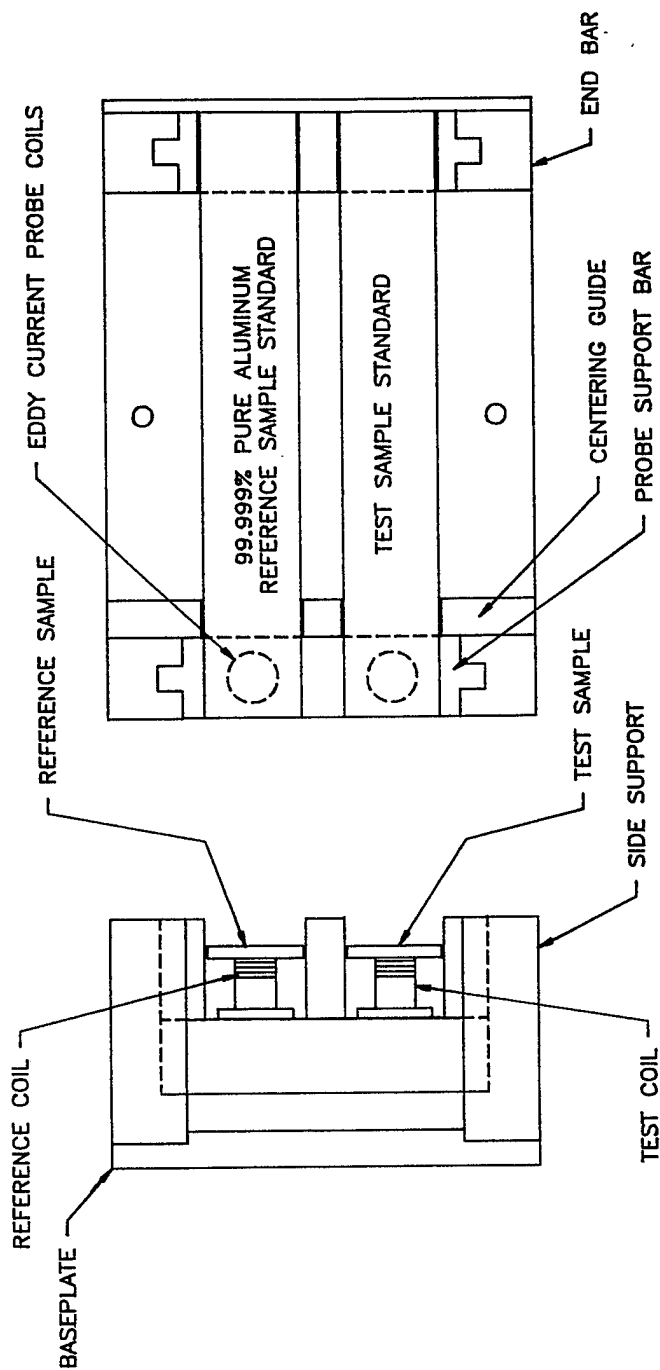
Figure 3.1 Schematic Drawing of Redesigned Apparatus (Top and Side Views).

21

3. Probe Coils

It became obvious early on that the probe coils would be the most difficult part of the eddy current monitoring system to redesign. The coils comprised three elements:

1) The bobbins or coil cores.
2) The wire used to wind the coils.
3) The wire insulation which prevented adjacent turns of wire from making direct contact with each other.

As with the apparatus framework, the bobbins were machined from the MAKOR ceramic. Once machined, however, great caution was required in winding the coils due to the brittle nature of the ceramic material.

In previous work [Refs. 1-3], the coils were wound with copper magnet wire having an operating temperature of 200° C. Since the coils were wound around Teflon bobbins, their maximum operating temperature was reduced to approximately 180° C. The coil wire and insulation were the Achilles heel in the attempt to design the apparatus for operation at 480-595° C. Although magnet wire and insulation are available that can operate at temperatures beyond 595° C, finding a combination that completely met the design criteria proved unsuccessful. The design criteria were as follows:

1) Operating temperature: 480-595° C.
2) Nominal inductance, L: 153 μH, each coil.
3) Coil ID = 0.20 cm (0.078 in).
4) Coil maximum dimensions: OD = 1.0 cm (0.394 in), height = 0.30 cm (0.118 in).

Numerous coil manufacturers were contacted and much time was spent attempting to locate a suitable wire and insulation combination. The following lists some of the more promising options researched, their maximum operating temperature, and the reason they were rejected:

1) Nickel-chromium magnet wire #30 with mica tape insulation (1000° C); rejected because the inductance requirement could not be met without exceeding maximum coil dimensions.

2) Nickel-chromium magnet wire #30, impregnated with a virtuous silica insulation (980° C); rejected because the insulation was too brittle and unwindable.

3) Nickel-chromium magnet wire #30 with a glass coating (800° C); rejected for the same reason as 1 above.

4) Copper magnet wire #28 with high temperature single nialaze insulation (260° C); rejected because it did not meet temperature requirements and was unavailable from manufacturers.

5) Copper magnet wire #30 with high temperature HAPTZ single nialaze insulation (220° C); rejected because it did not meet temperature requirements.

Unable to produce a coil which met all of the design criteria, option number five was selected since it was available, met three of the four criteria, and would extend the maximum operating temperature from the initial 180° C to 220° C. In addition, obtaining factory wound coils would eliminate the slight mismatch in behavior between the reference and test coils at elevated temperatures encountered by Hall [Ref. 3]. While these coils were being manufactured, the current work continued with the initial coils inserted into the MAKOR probe support bar.

C. REDESIGNED SENSOR SYSTEM

1. Apparatus Framework

The framework of the apparatus holds the probe coils and supports the samples as they lay (i.e., flat) on the coils. The framework was redesigned to hold samples of varying size and to monitor the aging process in other age hardenable alloys as well as aluminum alloys.

2. Probe Coils

The two probes are the basis for the eddy current monitoring system. By inducing eddy currents into the reference and test samples, the impedance of each coil changes and the bridge unbalance voltage, ΔV_{BCA}, increases or decreases accordingly. Because resistivity decreases throughout the aging process, the magnitude of the eddy currents induced in the test sample increases, impedance in the test coil increases, and ΔV_{BCA} will continually drop as the aging process progresses. Accordingly, the probe coils are the key to the monitoring system.

3. Bridge Carrier Amplifier/Filter (BCA)

The BCA, as designed by Christian [Ref. 17], measures the changes in inductive reactance between a reference and test coil connected in a bridge configuration. The bridge configuration is shown in Figure 3.2. Because the bridge output, ΔV_{BCA}, is synchronously demodulated, it can be "nulled" and will not be effected by the reactive elements in the bridge. That is, ΔV_{BCA} measurements can transition from a point above the nominal coil reactance value (21 Ω), through zero, to a point below the nominal reactance value [Ref. 17]. The BCA comprises an oscillator set at 5 volts RMS and 52 kHz, instrumentation amplifier, phase sensitive demodulator, amplifier/filter, and an RMS converter. Figure 3.3 shows a block diagram of the components of the BCA. The entire system has been optimized to be used with the eddy current coils. The system gain has been adjusted to provide an output range of −10 to +10 volts direct current (dc) [Ref. 17]. The following equation gives an expression for the system output [Ref. 1]:

$$\Delta V_{BCA} = \left(\frac{Z_1}{R_L + Z_1} - \frac{Z_2}{R_R + Z_2} \right) * V_i \qquad (3.1)$$

where Z_1 is the reference coil impedance, Z_2 is the test coil impedance, R_L and R_R are the resistances of the upper left and right legs of the bridge, and V_i is the input voltage [Ref. 2].

4. Digital Multimeter

The digital multimeter monitored ΔV_{BCA}, allowing the bridge to be nulled in preparation for a test run, and providing an interface for the input of ΔV_{BCA} to the data acquisition program [Ref. 3].

5. Data Acquisition Personal Computer (DAPC)

The DAPC stored the voltage, time, and temperature data files generated by the data acquisition program. All the voltage and temperature versus time plots were generated through the use of DAPC utility programs.
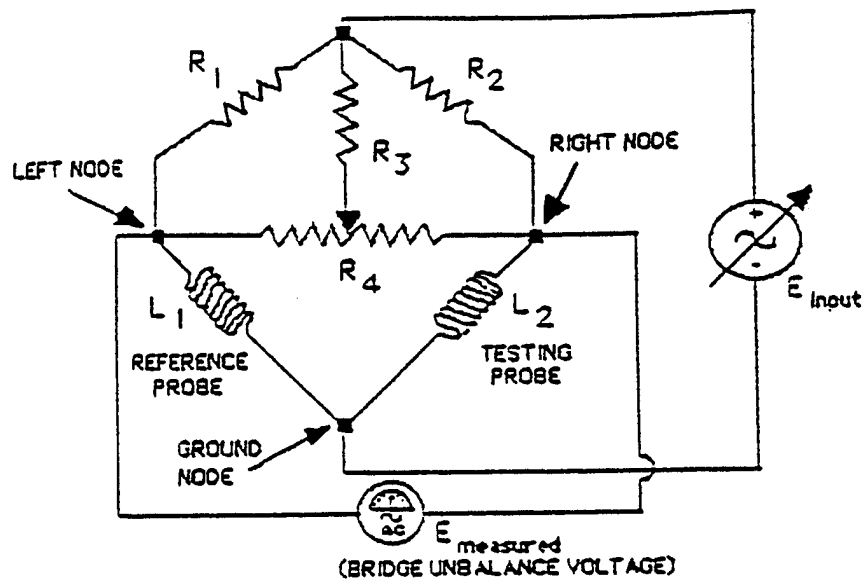
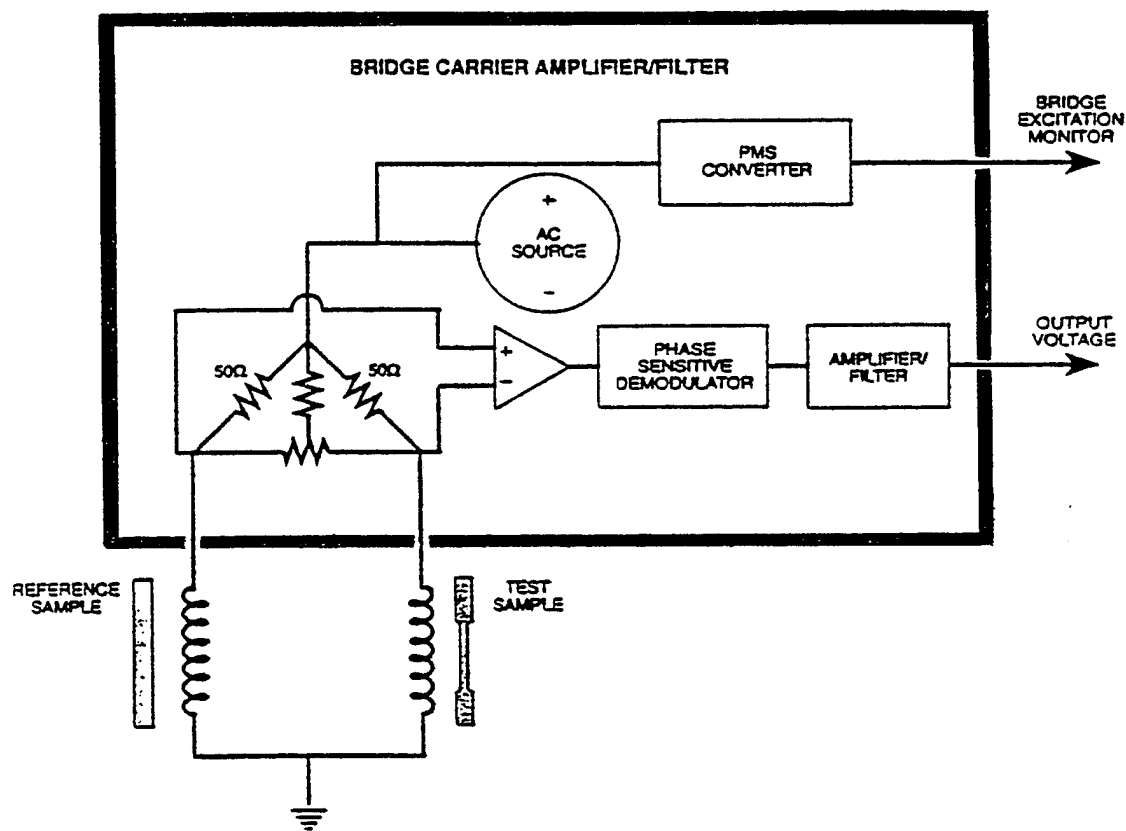Figure 3.2 Simplified Bridge Configuration. From Ref. [2].

Figure 3.3 Block Diagram of BCA Components. From Ref. [2].

IV. EXPERIMENTAL PROCEDURES FOR CALIBRATION AND MEASUREMENT

### A. STANDARD SAMPLE SELECTION AND PREPARATION

The objective of this work is to develop a system to continuously monitor the aging process by measuring the resistivity of an aging sample. Therefore, the output of the monitoring system, ΔV_{BCA}, must first be converted into a resistivity. This was accomplished by selecting test sample standards of known resistivities [Ref. 18], measuring the BCA output, ΔV_{BCA}, corresponding to each standard and developing an empirical equation relating ΔV_{BCA} to ρ. In resistivity measurements, one calibration standard must be above the highest value to be read and one below the lowest value to be read [Ref. 19]. Since the intent here is to measure the age hardening of 7075 Al, the standards in Table 2.2 were selected to satisfy the aforementioned criteria.

After selecting the test sample standard materials, coupons were then ground flat with a 600 grit abrasive paper, with the exception of the 6061 Al and 7075 Al standards which were already flat. Flatness was required to eliminate any variation in spacing between the surface of the coil and the test sample standards due to the lift-off factor described in Chapter II. Finally, the ground test sample standards were given either a full or a stress-relief anneal to eliminate the effects of plastic deformation on their resistivity values.

B. CALIBRATION RUNS

Data files consisting of ΔV_{BCA} and temperature readings were acquired for the test sample standards at test temperatures of 20° C, 50° C, 75° C, and 120° C. For each temperature, the following procedures were used to collect the data needed to generate calibration curves:

    (1) The convection oven was set at the desired temperature (20° C runs were performed at night so the ambient temperature was below 20° C) with the apparatus inside and two identical 99.999% pure aluminum samples on the reference and test coils. Figure 4.1 shows the apparatus inside the oven with the pure aluminum reference and test sample standards over the left and right coils respectively.
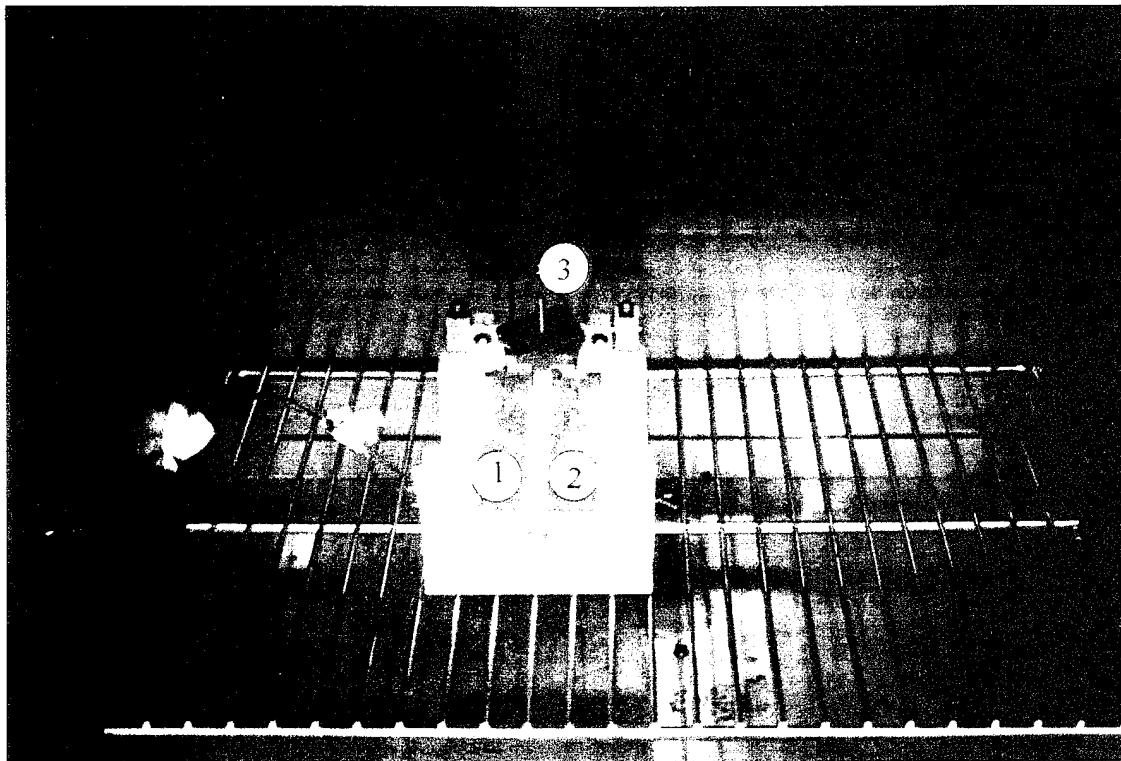
1. 99.999% pure aluminum reference sample standard on the reference coil.

2. 99.999% pure aluminum test sample standard on the test coil.

3. Thermocouple connection.

Figure 4.1 Photograph Showing Test Apparatus with 99.999% Pure Aluminum Reference and Test Sample Standards on the Left and Right Eddy Current Coils Respectively.

(2) When the thermocouples on both the reference and test samples indicated they had reached the desired equilibrium temperature, ΔV_{BCA} was nulled by adjusting the BCA.

(3) The data acquisition program was started, generating time versus ΔV_{BCA} and time versus temperature data files.

(4) The oven was opened immediately after starting the data acquisition program and thermocouples were lifted off the pure aluminum samples. The pure aluminum test sample standard on the right side was removed and replaced with the OF Cu test sample standard. The thermocouples were lowered back onto the samples and the over door closed.

(5) The temperature of both samples was monitored until both were at the equilibrium temperature (20° C, 50° C, 75° C, and 120° C) and data was taken for an additional one to two minutes. The data acquisition program was then stopped, the OF Cu sample was removed, and the pure aluminum test sample standard was replaced by repeating step 4.

(6) Steps 2-5 were repeated for the 1100 Al, 6061 Al, 7075 Al, and naval brass test sample standards, in that order.

C. AGING SAMPLE MEASURING PROCEDURE

The process for collecting data for an aged test sample was slightly different than the above procedure. First, the 7075 Al samples to be age hardened were solutionized at 480° C ($\pm$ 2° C) for 50 minutes and quenched into room temperature water. The sample was removed from the quench and dried for insertion into the convection oven. It should be noted that steps 1 and 2 were completed prior to removing the 7075 Al from the solutionizing oven. The test sample to be aged was then inserted into the apparatus using steps 3 and 4. The sample was allowed to age for a predetermined length of time before being removed and again replaced with the pure aluminum test sample standard. ΔV_{BCA} and temperature data was taken continuously during the time the sample was being aged. Figure 4.2 shows a photograph of some of the components that comprise the eddy current monitoring system.

V. RESULTS AND DISCUSSION

As previously discussed, the objectives of this thesis were twofold: (1), to redesign the apparatus to operate at higher temperature (as discussed in Chapter III); and (2), to develop a functional relationship between ΔV_{BCA} and resistivity (ρ).

A. ROOM TEMPERATURE (20° C) CALIBRATION

The eddy current monitoring system output, ΔV_{BCA}, clearly shows the same expected characteristics as the resistivity of the material. While such a result is useful, the aging process could not be quantitatively monitored without first converting ΔV_{BCA} to ρ. Again, the approach was to select several metals with known resistivities as sample standards and insert them into the apparatus to determine their corresponding ΔV_{BCA} values at various temperatures. With this data in hand, a functional relationship could be established and a calibration curve generated for each temperature of interest.

1. Initial Runs

Figure 5.1 (a) and (b) shows the first and second attempts to produce the data needed to generate the 20° C calibration curve. For the first run, the six test sample standards from Table 2.2 were measured in the apparatus without prior sample preparation. According to Table 2.2, the known resistivity values increase in ascending order from OF Cu to naval brass. Since ΔV_{BCA} is directly related to ρ, our values of ΔV_{BCA} should be similarly ordered. However, in Figure 5.1 (a), ΔV_{BCA} for 1100 Al is less than ΔV_{BCA} for pure Al and ΔV_{BCA} for naval brass is less than ΔV_{BCA} for 7075 Al. The reason for this is that the pure aluminum reference and test samples were not machined to the same degree of "flatness". When lowered onto the reference and test coils, the spacing between the sample standard and the coil surface was not the same. With greater spacing, lower eddy currents are generated in the metal sample standard, leading to a lower test coil impedance and higher ΔV_{BCA}. This condition is due to the lift-off factor described in Chapter II. In order to truly null ΔV_{BCA}, the pure aluminum
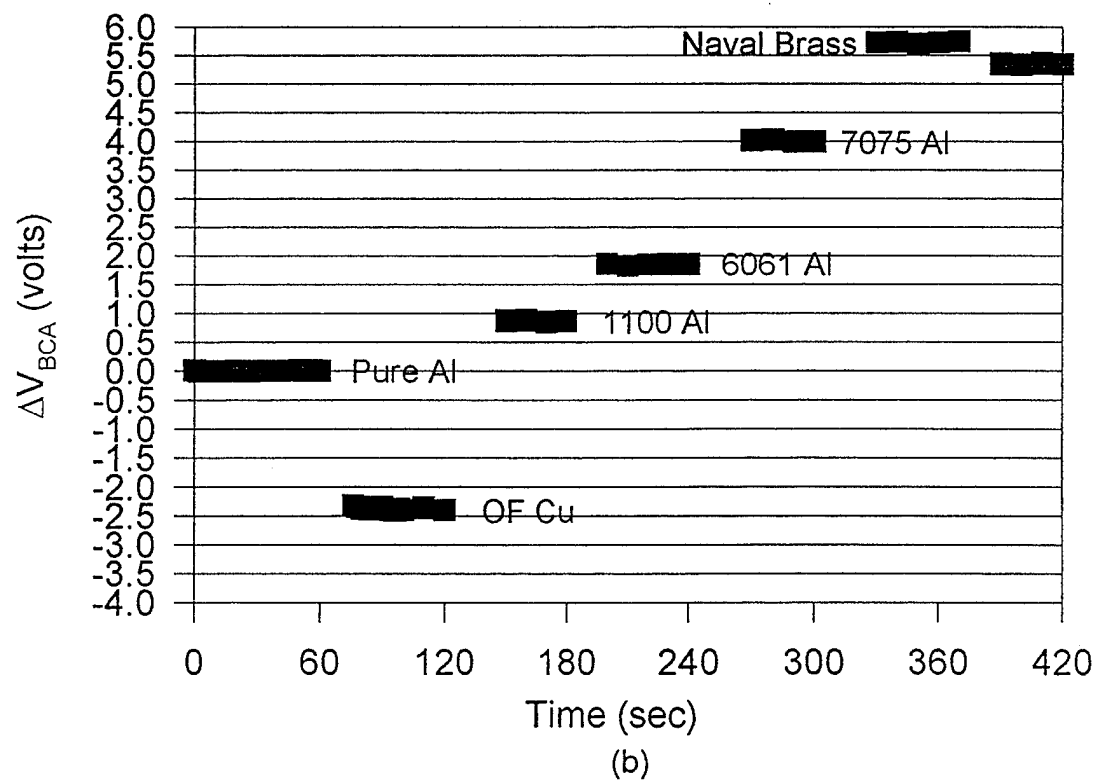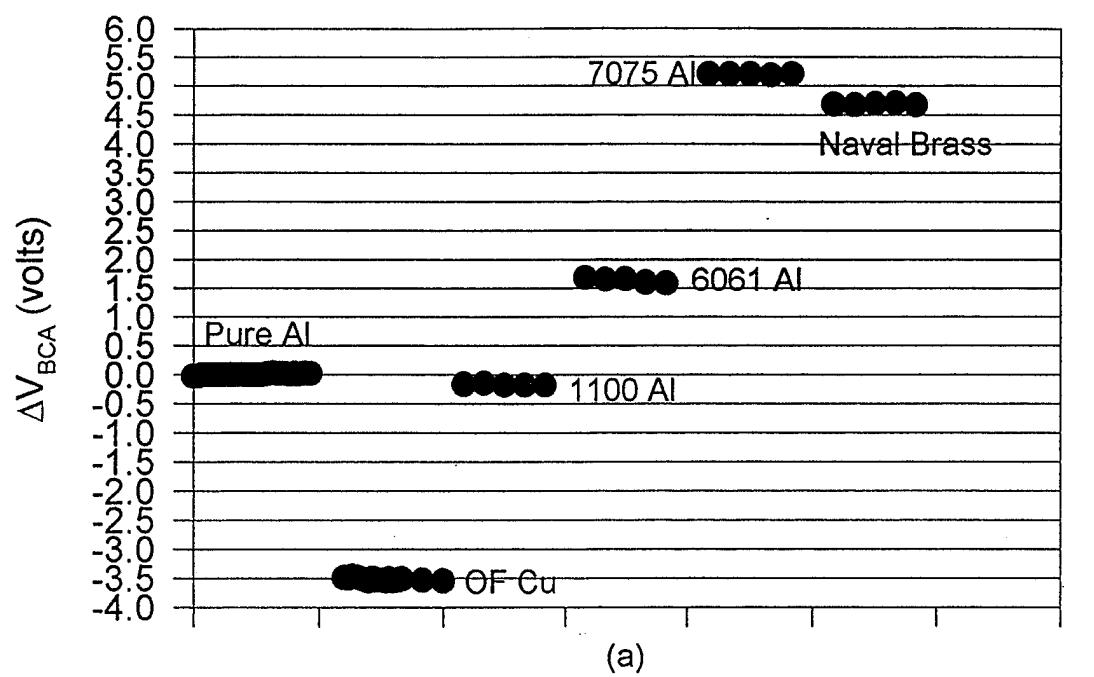
31

Figure 5.1 ΔV_{BCA} Values of Test Sample Standards at 20° C. (a) First Calibration Run. (b) Second Calibration Run.

reference and test sample standards must have the same degree of "flatness", i.e., the same degree of lift-off

Prior to run 2, the pure aluminum sample standards were gradually ground down to a 600 grit finish and checked for flatness until all were apparently flat. They were then fully annealed to remove any effects of plastic deformation on their resistivity. The six test samples were again tested in the apparatus and the results are shown graphically in Figure 5.1 (b). The ΔV_{BCA} values are now in an order that corresponds with their ρ values. However, notice the sudden drop in ΔV_{BCA} for naval brass at the end of run 2. This occurred after lifting the thermocouples, removing the naval brass test sample standard, then simply reinserting it into the apparatus. Upon closer visual inspection of the naval brass sample it was clear that it, too, was slightly warped and would require sanding to the same "apparent degree of flatness" as the pure aluminum samples to remove differences in lift-off. All test sample standards were then inspected by laying each on a flat straightedge and visually gauging their degree of flatness. It was determined that only the 6061 Al and 7075 Al samples were the same degree of flatness as the pure aluminum. The OF Cu, 1100 Al, and naval brass test sample standards were then ground so that all metal sample standards had the same apparent degree of flatness and would therefore experience the same lift-off factor. This time a stress relief anneal was performed to remove plastic deformation effects.

2. Final Calibration Curve

Figure 5.2 shows the ΔV_{BCA} values when all the standard samples have the same "apparent degree of flatness" and therefore no relative lift-off effects. With confidence that the lift-off factor had been eliminated from our data at 20° C, the mean value of ΔV_{BCA} (with standard deviation error bars) for each test sample standard was plotted versus $\Delta \rho$, where $\Delta \rho = \rho_{test} - \rho_{ref}$. The resulting curve is the 20° C calibration curve shown as Figure 5.3.
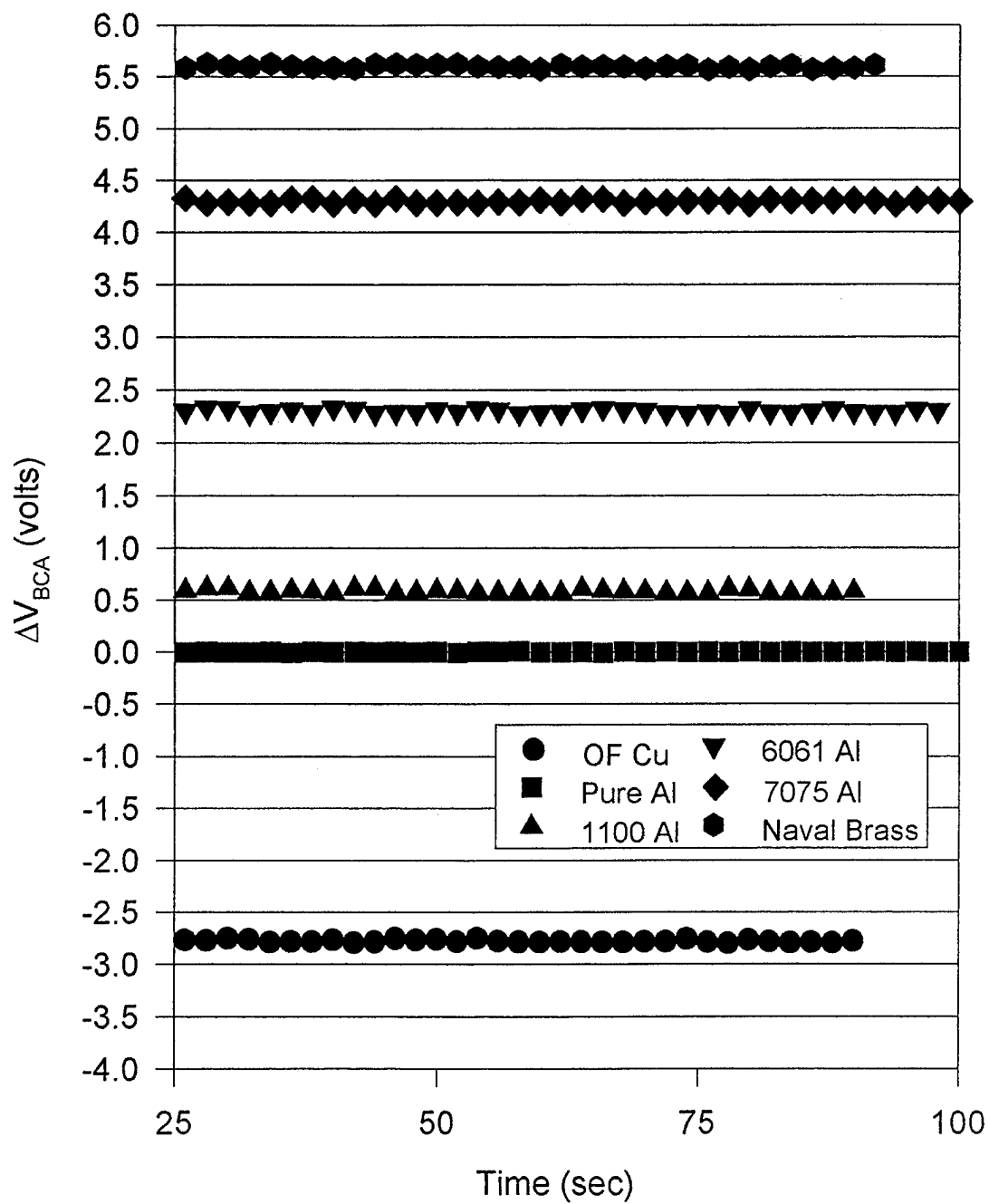
33

Figure 5.2 ΔV_{BCA} Values of Test Sample Standards for Final 20° C Calibration Run.
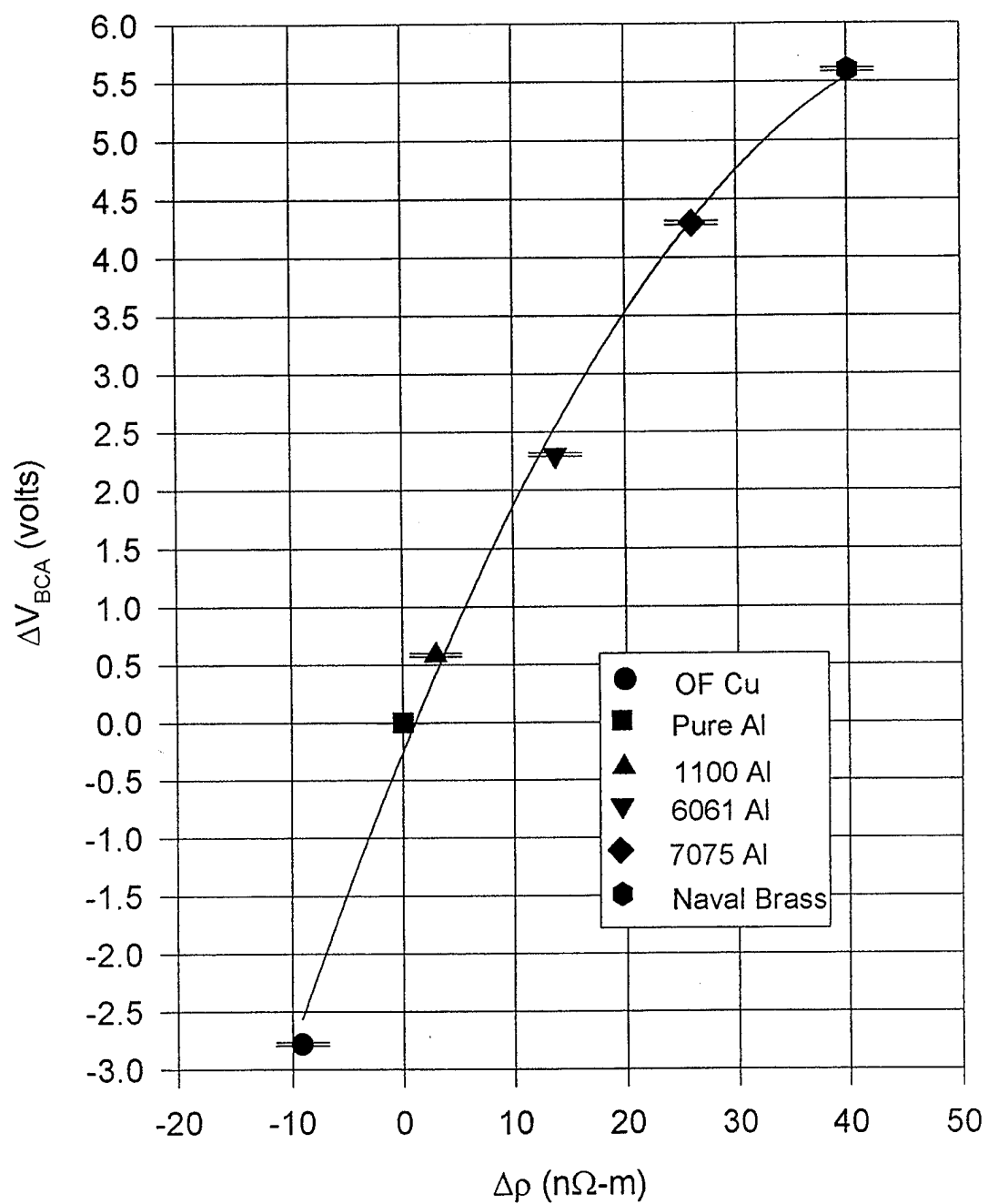
Figure 5.3 20° C Calibration Curve

B. ELEVATED TEMPERATURE CALIBRATIONS

1. Temperature Dependence

As shown in Figure 2.4, the resistivity of most metals is linear over a wide range of temperature. With this in mind, ρ was plotted versus temperature for the range 20° C to 120° C using equation 2.4 and the values of ρ and α (from the literature) for the six standard samples presented in Table 2.2 (the results are graphically presented in Figure 5.4). Note that the pure Al reference sample standard has a higher temperature coefficient and its resistivity is affected more by increasing temperature than five of the six test sample standards (the other test sample standard is also pure Al). Therefore, the value for ΔV_{BCA} for the system will decrease with temperature because the resistivity of the pure aluminum reference sample standard increases more than the resistivities of the test sample standards.

2. Calibration Curves for 50° C, 75° C, and 120° C

Following procedures identical to those for 20° C, ΔV_{BCA} values (mean) were produced for the six test sample standards at 50° C, 75° C, and 120° C. From the ρ versus temperature curve in Figure 5.4, ρ and $\Delta \rho$ were also determined. The values of ρ, ΔV_{BCA}, and $\Delta \rho$ are presented in Table 5.1. Using this data, additional calibration curves were generated. The 120° C calibration curve is shown in Figure 5.5 and again in Figure 5.6 where all the calibration curves have been plotted on the same axes.

Note that all the calibration curves have been fitted with second order polynomials rather than assuming a linear relationship for ΔV_{BCA} versus ρ. Recall that the system output equation for ΔV_{BCA} was provided in Chapter III as:

$$\Delta V_{BCA} = \left(\frac{Z_1}{R_L + Z_1} - \frac{Z_2}{R_R + Z_2} \right) * V_i \tag{3.1}$$

where R_L and R_R are resistive elements, each with a value of 50 Ω; Z_1 and Z_2 are the nominal reference and test coil impedances at 52 kHz, each with a value of 21 Ω; and V_i is the input voltage which equals a constant 5.0 volts. Consider a test sample to be replaced
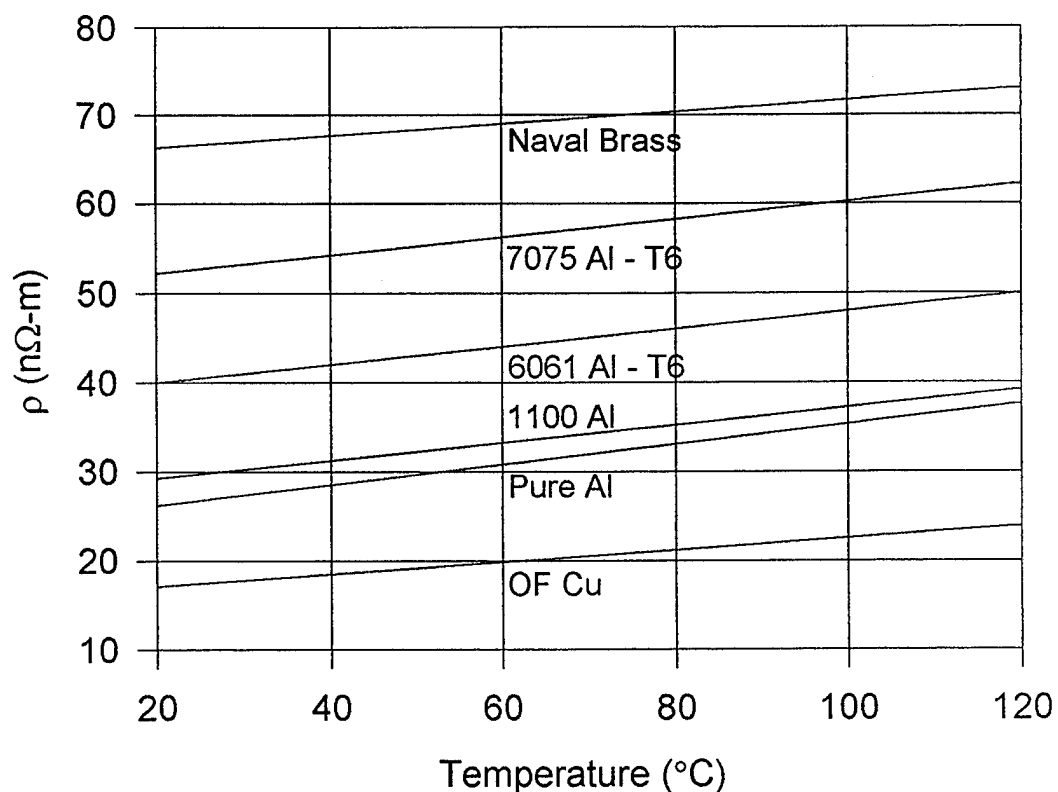
Figure 5.4 Electrical Resistivity Versus Temperature Showing the Temperature
Dependence for the Six Test Sample Standards.

Property	TEST SAMPLE STANDARDS					
	OF Cu	Pure Al	1100 Al	6061 Al	7075 Al	Nav.Brass
ρ_{20} (nΩ–m)	17.10	26.20	29.20	40.00	52.20	66.30
ρ_{50} (nΩ -m)	19.14	29.64	32.30	43.00	55.20	68.34
ρ_{75} (nΩ–m)	20.84	32.50	34.70	45.50	57.70	70.04
ρ_{120} (nΩ–m)	23.90	37.65	39.20	50.00	62.20	73.10
$\Delta V_{bca(20)}$ (volts)	-2.7801	0.0	0.5847	2.3051	4.2977	5.6004
$\Delta V_{bca(50)}$ (volts)	-2.9865	0.0	0.5534	2.0867	4.0789	5.0413
$\Delta V_{bca(75)}$ (volts)	-3.1963	0.0	0.5327	1.9788	3.7977	4.6454
$\Delta V_{bca(120)}$ (volts)	-3.5921	0.0	0.4716			4.1814
$\Delta\rho_{20}$ (nΩ–m)	-9.10	0.0	3.00	13.80	26.00	40.10
$\Delta\rho_{50}$ (nΩ–m)	-10.50	0.0	2.67	13.37	25.57	38.71
$\Delta\rho_{75}$ (nΩ–m)	-11.66	0.0	2.20	13.00	25.20	37.54
$\Delta\rho_{120}$ (nΩ–m)	-13.75	0.0	1.55	12.35	24.55	35.45

Table 5.1 ρ, ΔV_{BCA}, and $\Delta\rho$ for the Six Test Sample Standards at 20° C, 50° C, 75° C,
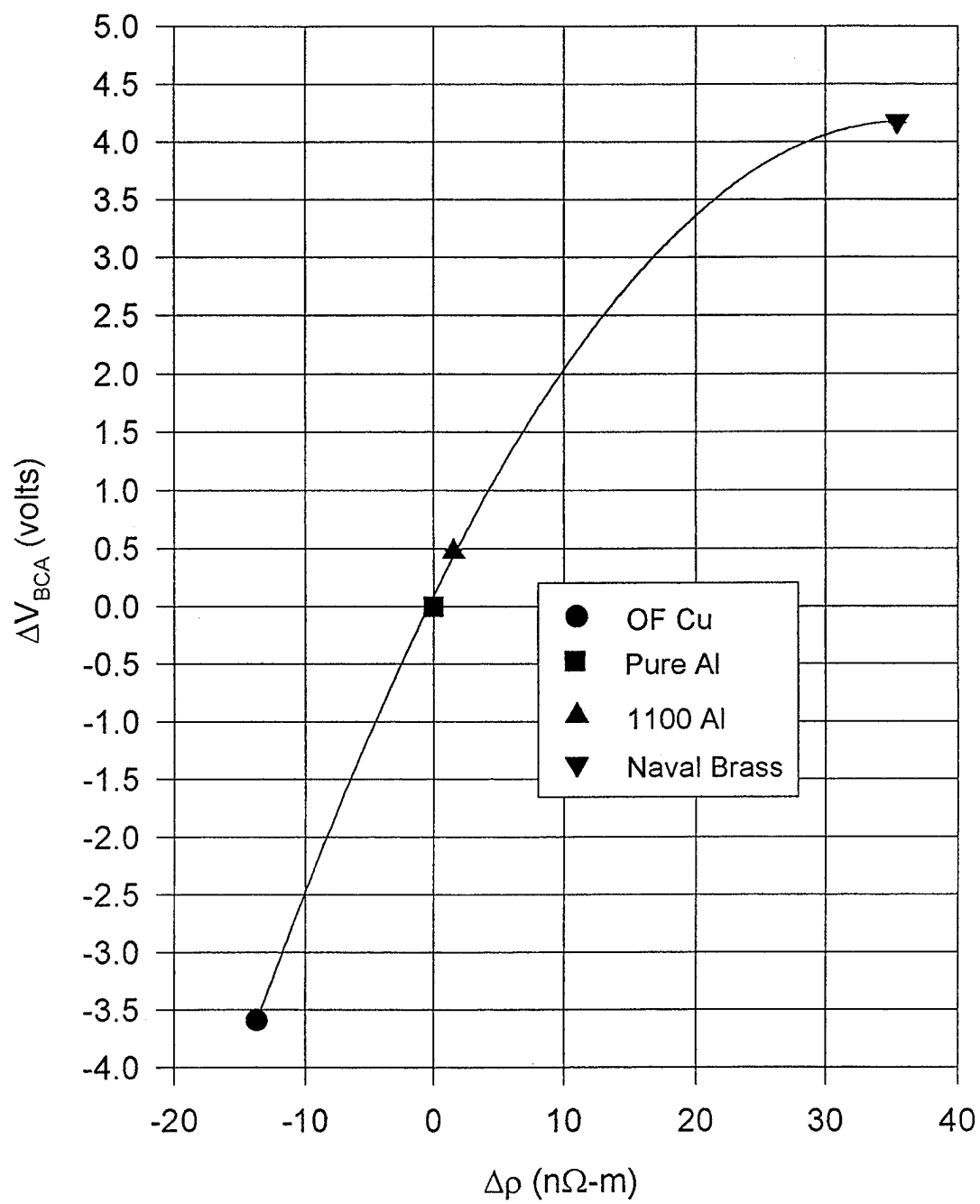and 120° C.

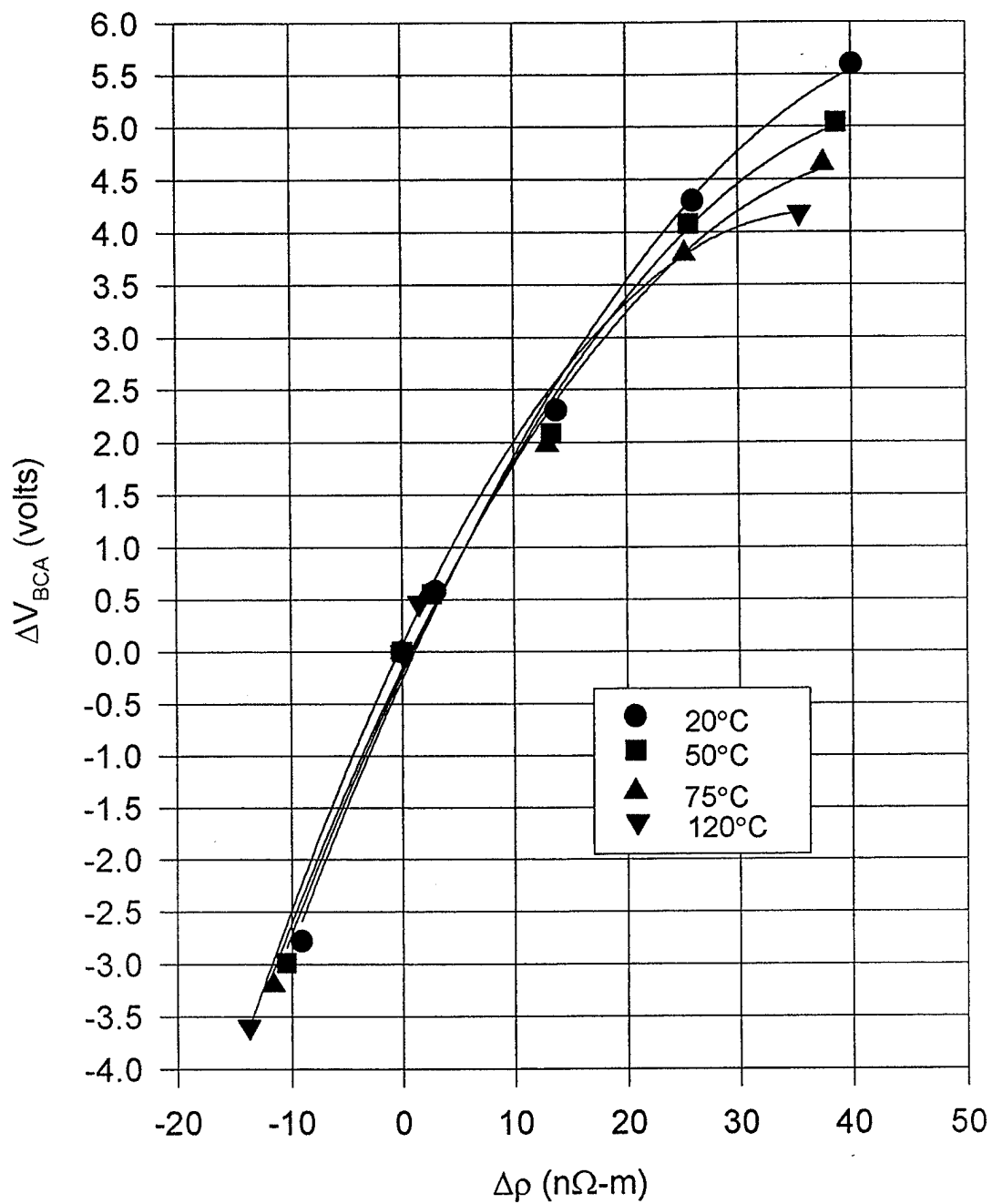Figure 5.5 120° C Calibration Curve.

Figure 5.6 20° C, 50° C, 75° C, and 120° C Calibration Curves.

with a sample of higher resistivity than pure aluminum, after the BCA is nulled with the two pure aluminum sample standards. Lower eddy currents are induced in the test sample (relative to the reference sample) and this means there is less current opposing the current flow in the test coil, resulting in a reduction in the test coil impedance, Z_2, with respect to the reference coil impedance, Z_1. Therefore, ΔV_{BCA} will increase but to a finite positive value. In fact, if the test sample were replaced with a sample having infinite resistivity, the test coil impedance would only be reduced to the nominal value of 21 Ω and ΔV_{BCA} would still reach a finite positive value. The converse is true if the test sample is replaced with a material of negligible resistivity, such as a superconductor. Higher eddy currents would be induced in the test sample, providing more opposition to current flow in the test coil. The test coil impedance would decrease, and ΔV_{BCA} would decrease to a finite negative value. Therefore, the relationship between ΔV_{BCA} and ρ is not linear and the data for each temperature was curve fitted with a second order polynomial. The resulting functional relationships determined for each temperature are as follows:

$$\Delta V_{BCA}(20) = -0.2549976905 + 0.2338699272(\Delta\rho) - 2.2258156930 \times 10^{-3}(\Delta\rho)^2 \quad (5.1)$$

$$\Delta V_{BCA}(50) = -0.1931071399 + 0.2274901785(\Delta\rho) - 2.4171904384 \times 10^{-3}(\Delta\rho)^2 \quad (5.2)$$

$$\Delta V_{BCA}(75) = -0.1342220687 + 0.2193186718(\Delta\rho) - 2.4916181212 \times 10^{-3}(\Delta\rho)^2 \quad (5.3)$$

$$\Delta V_{BCA}(120) = 0.0675426881 + 0.2244697749(\Delta\rho) - 3.0577906350 \times 10^{-3}(\Delta\rho)^2 \quad (5.4)$$

The curves will be used to convert ΔV_{BCA} to $\Delta\rho$ when the apparatus is used to monitor the isothermal aging process in 7075 Al.

C. ISOTHERMAL AGING RUNS (120° C)

In previous work, the eddy current monitoring system was used to generate plots of ΔV_{BCA} versus aging time. The resulting curves were then analyzed, but no direct correlation was made between ΔV_{BCA} and ρ. In this work, the calibration curves at 20° C and 120° C will be utilized to apply a lift-off correction (LOC) to the aging test sample and to directly convert ΔV_{BCA} to $\Delta\rho$. When a test sample has been solutionized, the

subsequent quench to room temperature causes distortion or warpage. This warpage causes variations in the "flatness" of the quenched test sample relative to the "flatness" of the test sample standards used to generate the calibration curves. A correction must be applied to the resulting variation in resistivity due to lift-off prior to using the calibration curves to convert ΔV_{BCA} to $\Delta \rho$.
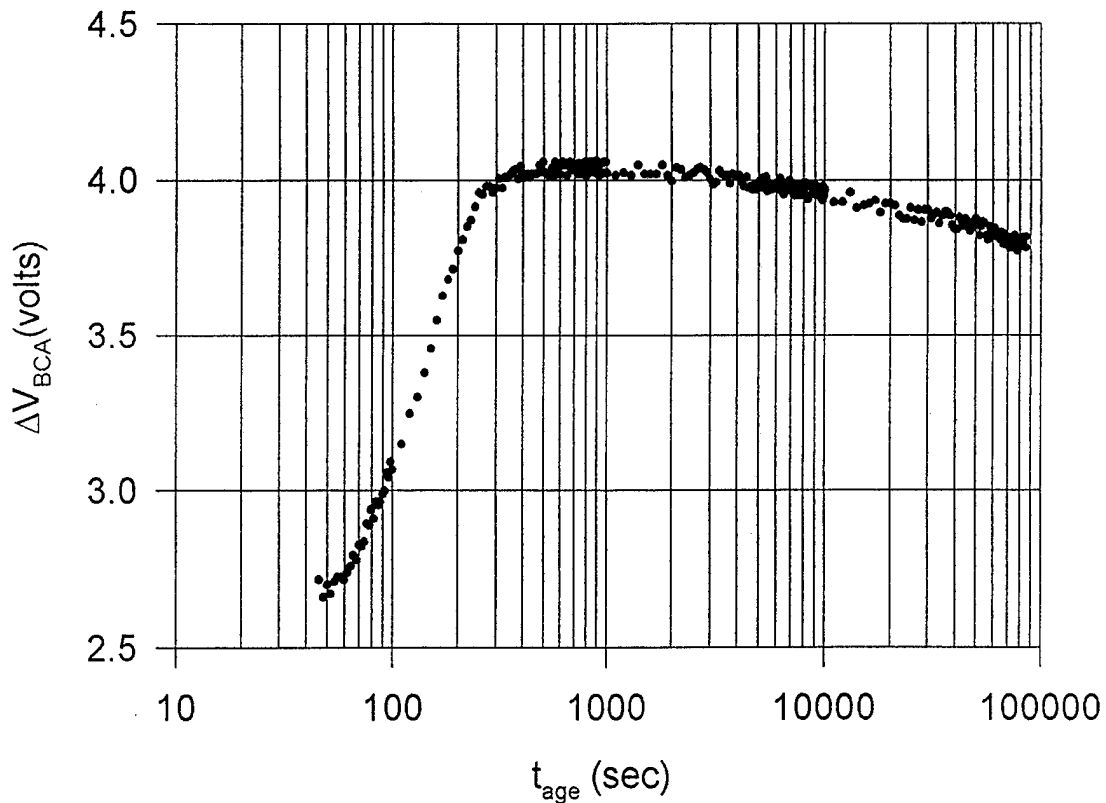
1. System Output

The data acquisition program for the eddy current monitoring system generates data files for ΔV_{BCA}, reference and test sample temperature, and time. By plotting ΔV_{BCA} and temperature versus time, the behavior of each can monitored the as the aging process progresses. The temperature and ΔV_{BCA} versus t_{age} plots shown in Figure 5.7 (a) and (b) were obtained utilizing the aging sample measuring procedure described in Chapter IV.

The temperature versus t_{age} plot shows that the temperature of the pure aluminum reference sample initially drops due to opening the oven door and then rises to its equilibrium temperature, while the test sample temperature continually rises from its as-quenched temperature to equilibrium at the test temperature. As with the data recorded by Hall [Ref. 3], the test sample reaches equilibrium with the oven temperature at about 500 to 600 seconds. This also corresponds to the time that ΔV_{BCA} reaches its peak value. This is seen by examining the ΔV_{BCA} versus t_{age} plot in Figure 5.7 (b).

The ΔV_{BCA} versus t_{age} curve rises steadily to the point that the reference and test samples are in thermal equilibrium, and then begins to steadily decrease. This is for several reasons. First, the resistivity of the 7075 Al test sample at its quenched temperature is greater than the resistivity of the pure Al test sample at 120° C resulting in an increase in ΔV_{BCA} according to Equation 3.1. As the 7075 Al test sample increases in temperature, thermal vibrations further increase its resistivity (exceeding the decrease in resistivity caused by the solutes being removed from solution due to the aging process) and ΔV_{BCA} continues to rise until the test sample reaches the equilibrium temperature. At this point the resistivity decrease due to the aging process takes over and ΔV_{BCA} decreases until the test sample is removed from the apparatus.

41
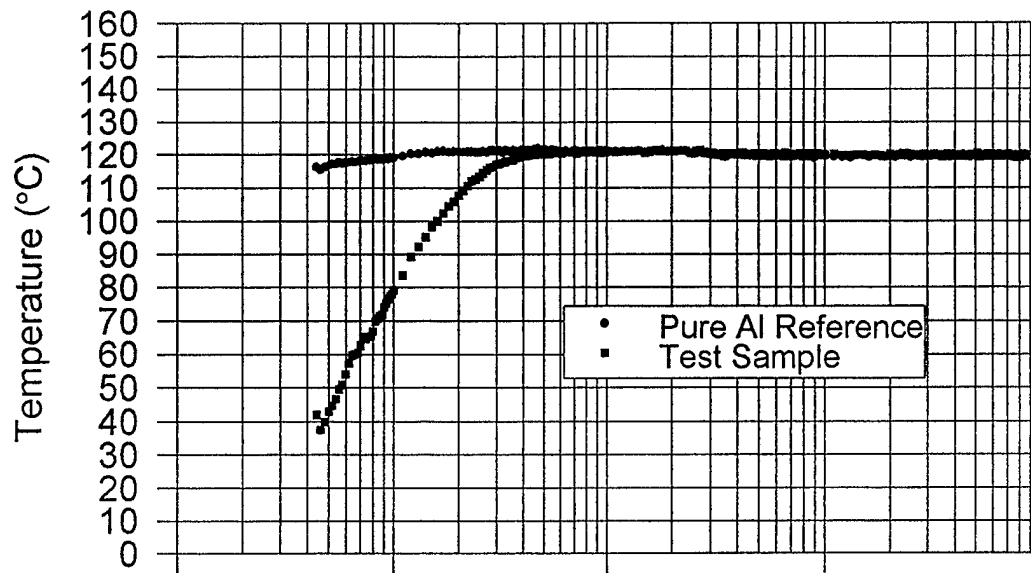
Figure 5.7 System Output Versus Aging Time for 120° C Isothermal Aging Run.
(a) Temperature Versus Aging Time. (b) ΔV_{BCA} Versus Aging Time.

42

2. Lift-Off Correction (LOC)

The relative lift-off between the standard samples could be eliminated by ensuring that each had the same degree of " apparent flatness". It was not possible, however, to subject the quenched 7075 Al samples to the same preparations to ensure flatness prior to insertion into the apparatus (aging commences even at room temperature). Therefore an LOC would have to be applied before using the calibration curves to convert ΔV_{BCA} to ρ.

The sample whose aging curve appears in Figure 5.7 (b), was removed at 24 hours. Subsequent hardness tests revealed that T6 tempering had been achieved. The ΔV_{BCA} data was replotted from the time of maximum ΔV_{BCA} (about 500 sec) to the time of removal and a second-order polynomial curve fit was applied to the data. This is shown as the uncorrected curve of Figure 5.8. Since the 7075 Al aging test sample and the 7075 Al test sample standard are both aged to the T6 temper, their resistivities and ΔV_{BCA} values should be identical except for the variation due to lift-off (both the sample and the standard were from the same sheet of material). Since this variation would be constant throughout the aging process, once identified, it could be added or subtracted as necessary to correct the aging curve for lift-off relative to the test sample standards. Using the curve fit of the uncorrected data of Figure 5.8, the value of ΔV_{BCA} is read at the time corresponding to T6 tempering or the 24 hour point ($\Delta V_{BCA} = 3.795$ volts). Now, taking $\Delta\rho_{120}=24.55$ nΩ-m from Table 5.1 and inserting this value into Equation 5.4, a value for ΔV_{BCA} equal to 3.735 volts is obtained for this test sample standard. Taking the difference between the test sample standard and the as-tested aging sample gives us the desired lift-off correction, LOC = 3.735-3.795 = -0.060 volts. This LOC was then systematically applied to each data point of the uncorrected curve resulting in the corrected curve, which can now be converted directly to resistivity using Equation 5.4. Figure 5.9 shows the uncorrected and corrected data for the 24 hour aging run at 120° C.

A second order polynomial curve fit was then applied to the corrected data of the 24 hour aging run and is shown in Figure 5.8. This data will be used later to correct
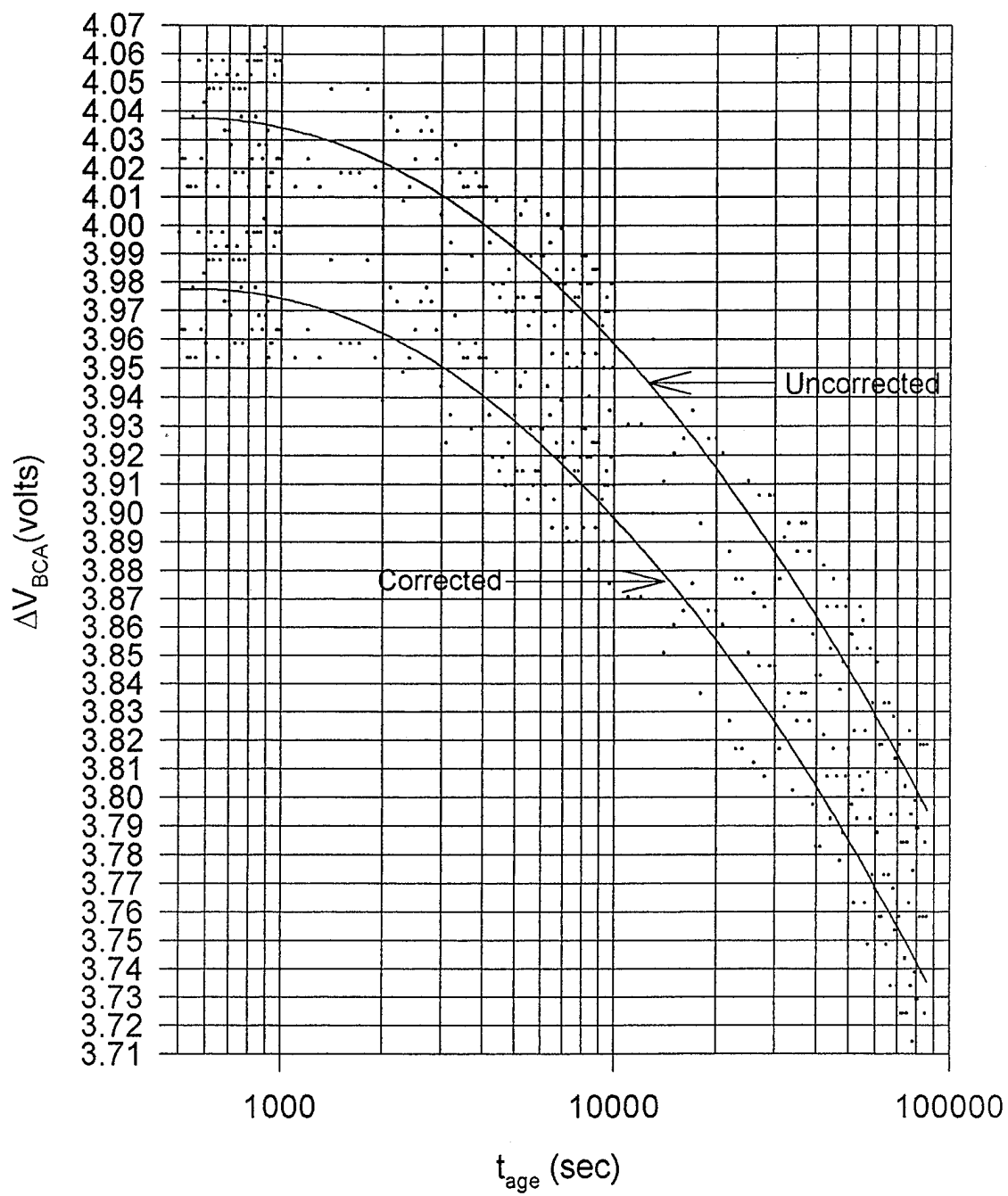
Figure 5.8 Uncorrected and Corrected Second Order Polynomial Curve Fits for 24-hour Aging Run at 120° C.
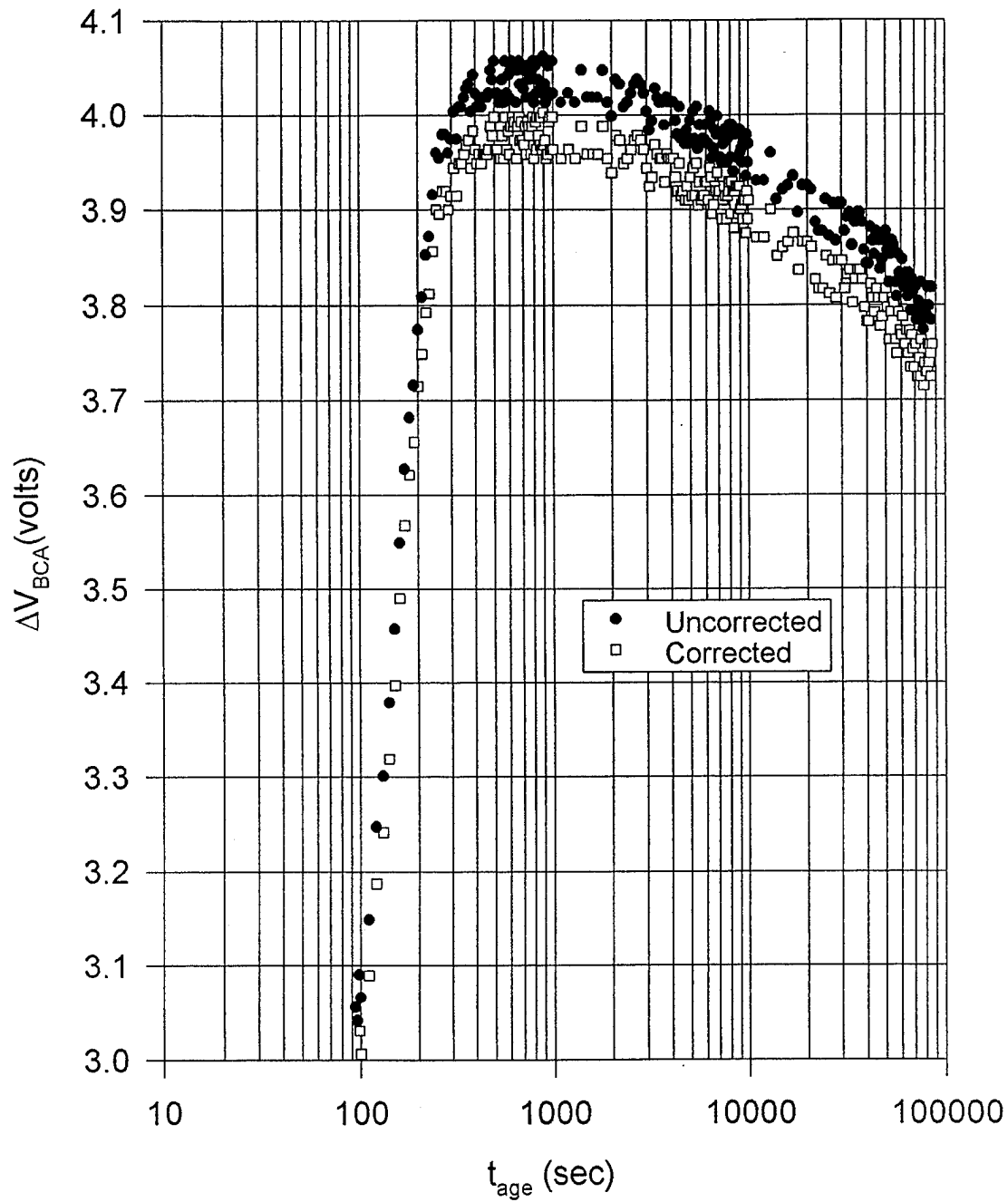
Figure 5.9 Uncorrected and Corrected ΔV_{BCA} Versus Aging Time Plots for 24-hour Aging Run at 120° C.

45

subsequent 120° C aging runs for various times in order to develop a relationship between material property behavior and aging time.

3. Material Property Behavior With Increasing Aging Time

It was shown by Hall [Ref. 3] that the aging curves of 7075 Al, when normalized to the peak value of ΔV_{BCA}, all lie on top of one another. The data obtained in this work demonstrated this to be true as well, as evidenced by Figure 5.10 (a) which shows the aging curves for five different aging times at 120° C. When normalized to the peak value of ΔV_{BCA}, the curves fall on top of each other. Using this information, the values of ΔV_{BCA} were read from the corrected curve in Figure 5.8 for 500 sec, 1 hour, 5 hours, 10 hours, 17 hours, and 24 hours of aging. Substituting these values into equation 5.4 allows solution for $\Delta \rho$ at 120° C. Since $\rho_{7075} = \rho_{pure\ Al} + \Delta \rho$, the data from Table 5.1 may be employed to determine the resistivity of 7075 Al at 120° C. Finally, the resistivity at 20° C can be computed using Equation 2.4. In Figure 5.11 (a) the resistivity for 7075 Al at 20° C is plotted versus t_{age} to show the relationship of resistivity versus time, which is the additional step needed to quantify the output of the monitoring system and which was lacking in previous work on this subject [Refs. 1-3]. As evident in Figure 5.11 (a), resistivity decreases with increasing aging time, as expected.

It is of great interest to see the relationship of strength or hardness versus aging time in order to develop a true "aging curve". The 7075 Al samples aged at 120° C for 1 hour, 5 hours, 10 hours, 17 hours, and 24 hours were immediately quenched in water to room temperature and placed in a freezer at 0° C following their aging runs in the eddy current monitoring apparatus. They were removed at a later date and five hardness tests were carried out for each sample. The mean hardness for this data was plotted versus aging time and the aging curve in Figure 5.11 was generated showing the increase in hardness with increasing aging time. The hardness reaches a value of 92 HRB at 24 hours (i.e., peak aging time). It is expected that the hardness would begin to drop at a time soon after the peak aging time. As the precipitates begin to coalesce and coarsen, dislocation motion is no longer as severely impeded. Rather, they are able to loop around

46

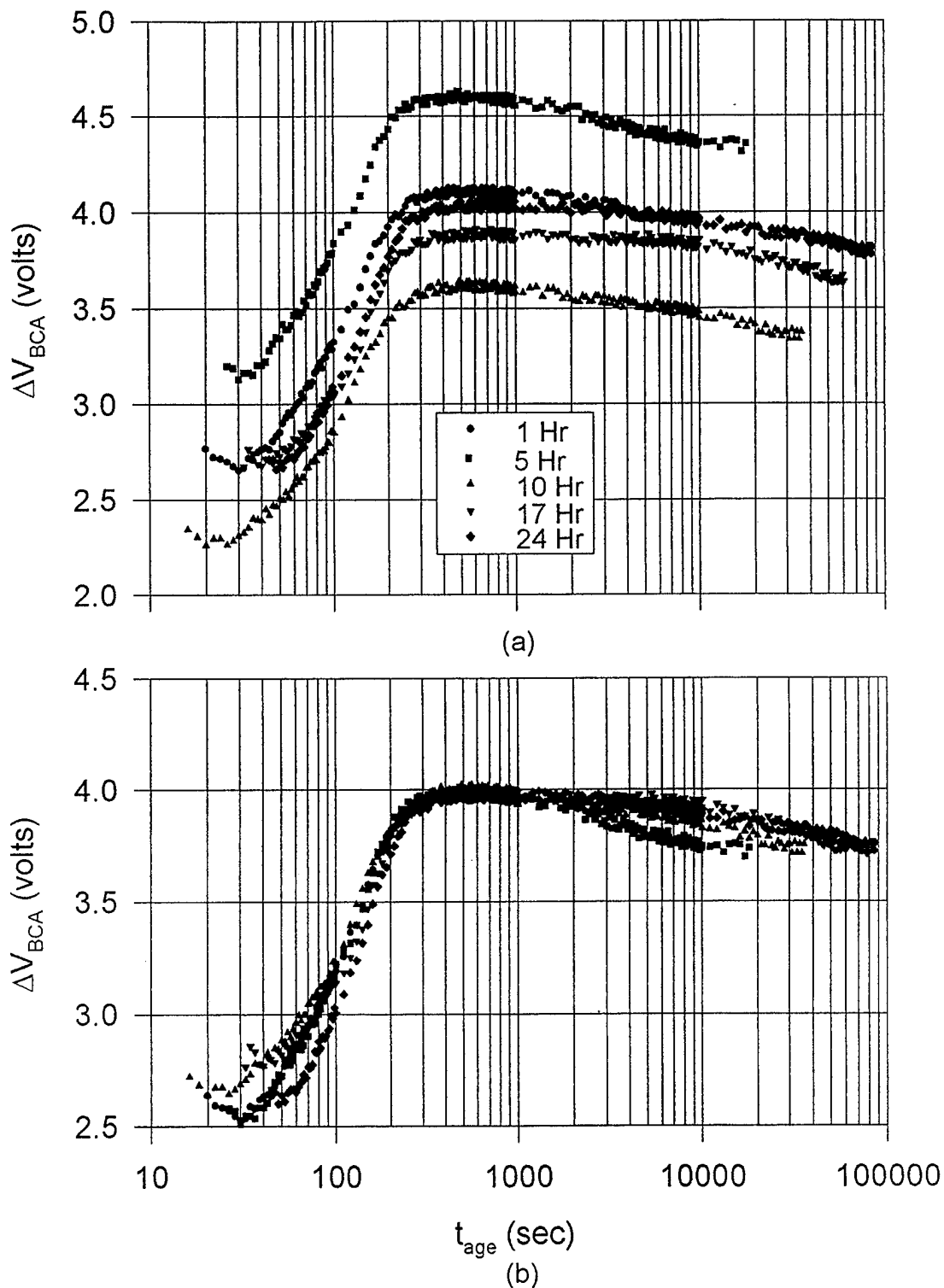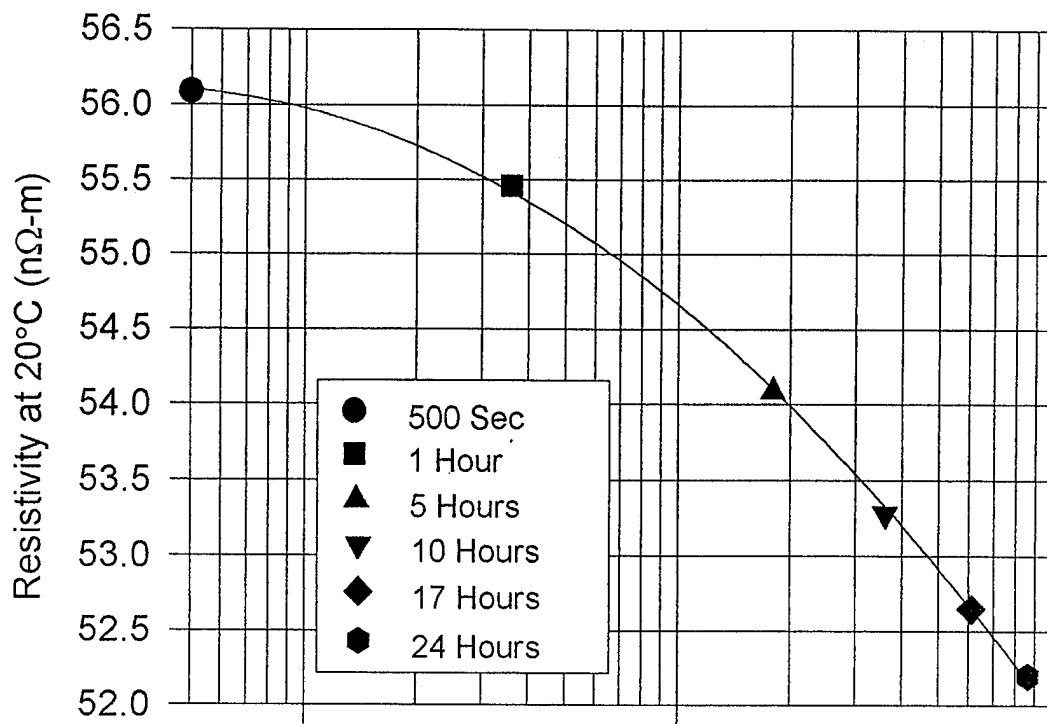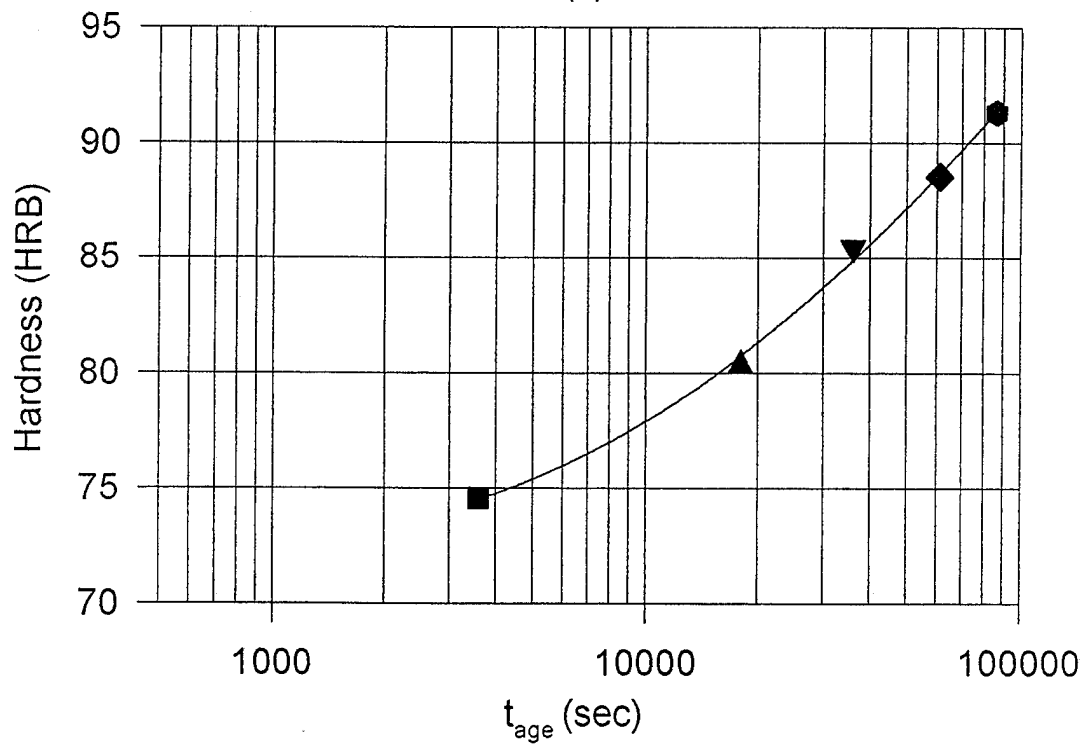Figure 5.10 ΔV_{BCA} Versus Aging Time Plots for Five Different Aging Times at 120° C. (a) Uncorrected Curves Which Show the Effect of Lift-off. (b) Corrected Curves Which have had Lift-off Correction (LOC) Applied.

47

Figure 5.11 Resistivity and Hardness Versus Aging Time for 7075 Al at 20° C.
(a) ρ Versus t_{age}. (b) Aging Curve.

48

the precipitates which tend to grow further apart due to a reduction in surface area associated with the coarsening.

With a clear understanding of the relationship among ΔV_{BCA}, $\Delta \rho$, and the LOC, the real-time monitoring system and LOC can be used to determine the appropriate moment to terminate the heat treating process. By identifying the peak value of ΔV_{BCA} when the reference and test samples reach the equilibrium temperature, it can be compared to the peak value of the corrected aging curve and the LOC determined. The LOC can then be applied in real-time to each data point as it is generated until the ΔV_{BCA} corrected value reaches the value from the 120° C calibration curve for peak-aged 7075 Al. At such a point the heat treating would be terminated. An intelligent control system could be employed to monitor the peak value of the aging curve or the decreasing slope of the aging curve to determine if the peak-aged voltage or resistivity criteria will be met, and terminate the heat treating when the criteria is satisfied or when it is determined the criteria will not be met. Such intelligent processing would allow the narrowing of engineering specifications for heat treated materials and improve the reliability of engineering structures using such heat treated materials.

4. Conductivity Versus Hardness Correlation

Figure 5.12 shows the relationship between conductivity versus hardness. From the physical behavior of hardness, it is clear that there is not a one-to-one relationship between the two. Hardness will eventually decrease while conductivity will continue to increase. It is noteworthy that the conductivity value obtained here for peak-aged 7075 Al, 33% IACS, corresponds exactly to the handbook value [Ref. 9]. Any control system used in the monitoring of the aging process must be capable of distinguishing between the same value of hardness for two different values of conductivity or resistivity if hardness data is to be part of the input to an intelligent control system.
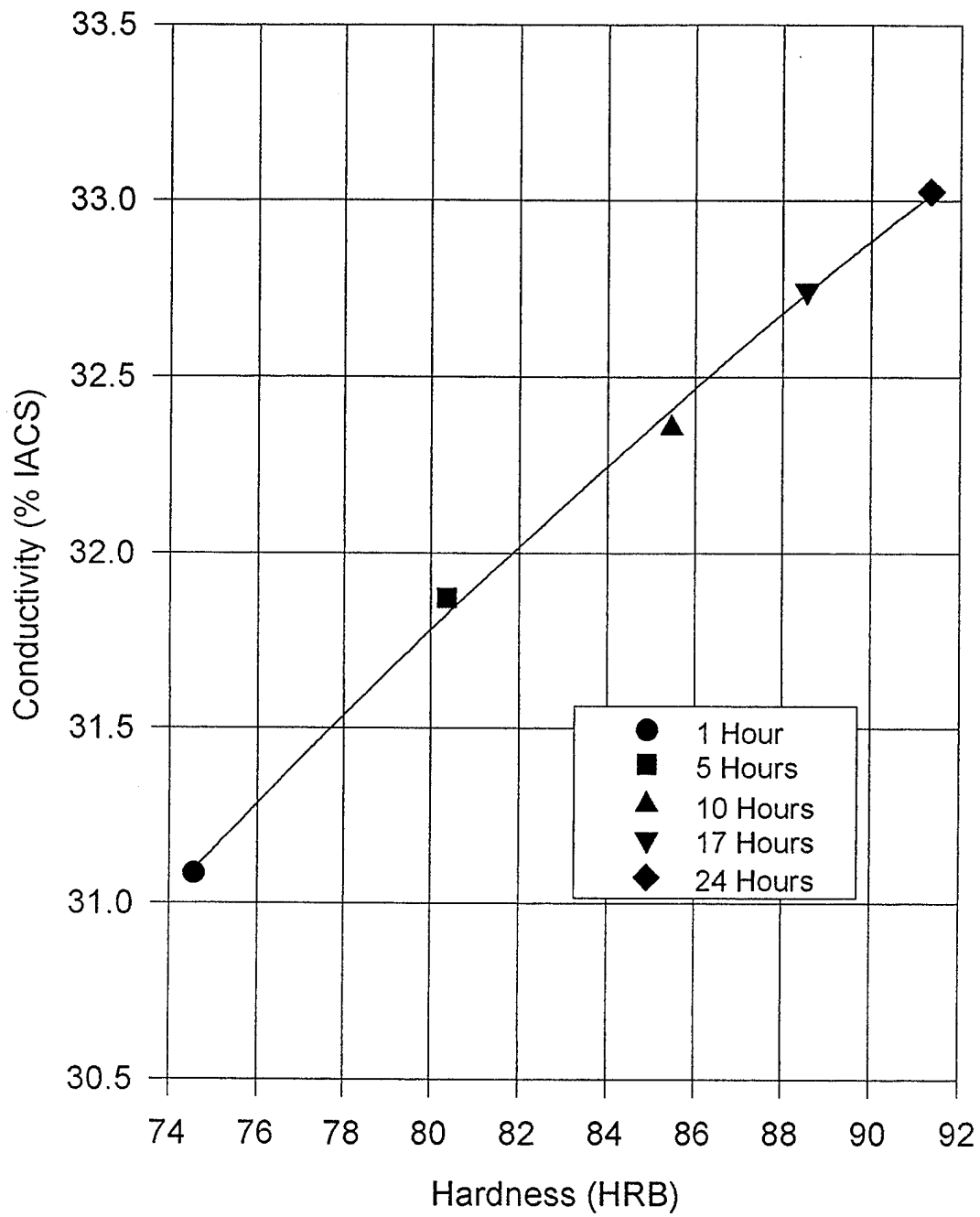
49

Figure 5.12 Curve Showing the Relationship of Conductivity Versus Hardness.

50

VI. CONCLUSIONS AND RECOMMENDATIONS

The conclusions and recommendations that follow were drawn as a result of this thesis project.

A. CONCLUSIONS

1. Test Apparatus Design

Numerous test runs were carried out flawlessly with the new ceramic apparatus and it performs its intended function extremely well. Even at elevated temperatures, the insertion and removal of aging samples was quick and easy.

2. Coil Performance

The initial coils were more than adequate for monitoring isothermal aging. Although the coils were not identical, the variation in system response with increasing temperature observed by Hall [Ref. 3] was eliminated by nulling the BCA when the reference and test coils reached thermal equilibrium with the convection oven.

3. Lift-Off Factor

Lift-off effects were eliminated in metals used as calibration standards by ensuring each had the same "apparent flatness". In aging test samples, distortion due to quenching caused a lift-off effect in ΔV_{BCA} measurement. This tended to cause higher than expected values of ΔV_{BCA}. By applying a lift-off correction, the calibration curves could then be used to convert ΔV_{BCA} to $\Delta \rho$.

4. Calibration Curves

Metals with known values of resistivity were measured in the system. By plotting their resulting ΔV_{BCA} values versus $\Delta \rho$, the functional relationship (at the specific temperature) could be used to convert any ΔV_{BCA} value to $\Delta \rho$.

51

5. Real-Time Monitoring of Aging Process

The eddy current monitoring system can be used to continuously measure resistivity throughout the aging process. Understanding the relationships among ΔV_{BCA}, $\Delta \rho$, and lift-off is the key to unlocking the full potential of the system. The voltage output, converted to resistivity, can provide real-time feedback to a control system that intelligently uses this information to terminate the heat treating process when the alloy attains peak aging. Alternatively, the system could be used as a scientific device to further study the effects of aging. Aging curves can be generated real-time, making the eddy current monitoring system ideal for laboratory experiments.

B. RECOMMENDATIONS

1. Probe Coils

New factory wound probe coils that would increase the system operating temperature to 220° C have been ordered. The more closely matched coils will promote multi-stage heat treatment testing which was not feasible in this work. Also the use of anodized aluminum as a coil winding material should be further researched. Since aluminum has a melting temperature of 660.4° C [Ref. 6], a system incorporating anodized aluminum coils could be used to monitor the aging process in titanium alloys.

2. Test Sample Geometry

A test sample geometry that limits the effects from lift-off should be used in future testing. Thicker and shorter samples would distort less during quenching and limit lift-off effects. By reconfiguring the current apparatus, samples with lengths down to three inches and virtually any thickness can be accommodated. The width should remain at one inch for the current coil diameter to avoid any edge effects. A design change to the apparatus allowing the test sample to rest entirely on the coil surface alone (versus support at both ends) would limit lift-off effects even more.

3. Sample Standards

Obtaining a magnesium test sample standard (ρ = 46 nΩ-m) to replace the 6061 Al (ρ = 41 nΩ-m) and 7075 Al (ρ = 53 nΩ-m) is advisable. Pure magnesium is not age hardenable and would eliminate any possibility of precipitation effects from the calibration data.

4. High Temperature Oven

The location of a high temperature oven to be used in the monitoring of age hardening in titanium alloys is critical. The oven must have at least two openings for thermocouple and coil connections and be large enough to provide adequate room to insert and remove test samples easily.

LIST OF REFERENCES

1. Esarey, J.G., *Continuous Measurement by Eddy Current Methods of Age Hardening in Aluminum Alloys*, Master's Thesis, Naval Postgraduate School, Monterey, California, September, 1992.

2. Mata, S.G., *Continuous Measurement of Aging Response in Aluminum Alloys by Eddy Current Methods*, Master's Thesis, Naval Postgraduate School, Monterey, California, December, 1993.

3. Hall, R.A., *Sensor Development for Intelligent Processing of Age Hardenable Aluminum Alloys*, Master's Thesis, Naval Postgraduate School, Monterey, California, March, 1995.

4. Callister, W.D., *Material Science and Engineering, An Introduction*, 2nd Edition, John Wiley & Sons, Inc., 1991.

5. Rosen, M., Horowitz, E., Swartzendruber, L., Fick, S., Mehrabian, R., "The Aging Process in Aluminum Alloy 2024 Studied by Means of Eddy Currents," *Materials Science and Engineering*, vol. 53, pp. 191-198, 1981.

6. Smith, W.F., *Foundations of Materials Science and Engineering*, 2nd Edition, McGraw-Hill Inc., 1993.

7. *Metals Handbook*, 9th Edition, Vol. 17, edited by Lampman, S.R., et. al., American Society for Metals International, 1989.

8. Van Vlack, L.H., *Elements of Materials Science and Engineering*, 5th Edition, Addison-Wesley Publishing Company, 1985.

9. *ASM Handbook*, vol. 2, Formerly 10th Edition, Metals Handbook, American Society for Metals International, 1992.

10. Hertzberg, R.W., *Deformation and Fracture Mechanics of Engineering Materials*, 3rd Edition, John Wiley & Sons, 1989.

11. Smallman, R.E., *Modern Physical Metallurgy*, Butterworth & Co. Ltd, 1985.

12. Rosen, M., "Eddy Current Analysis of Precipitation Kinetics in Aluminum Alloys," *Metallurgical Transactions A*, vol. 20A, pp. 605-610, April 1989.

13. Rummel, W.D., Arbegast, W.J., *Characterization of 2014, 2219, 6061, and 7075 Aluminum Alloy Heat Treatment Response by Eddy Current Conductivity, Hardness and Mechanical Properties*, American Society for Non-Destructive Testing, Inc., 1980.

14. Seltzer, D.D., *Correlation of Conductivity to Mechanical Properties of Age-Hardenable Aluminum Alloys Using Eddy-Current Methods*, "Proceedings for the Fifth International Conference on Non-Destructive Testing," Department of Energy, Mines and Resources, pp.283-291, 1969.

15. *ASM Handbook*, vol. 4, American Society for Metals International, 1991.

16. Shinskey, F.G., *Process Control Systems, Application, Design, and Tuning*, Third Edition, McGraw-Hill Publishing Company, 1988.

17. Private communication between Tom Christian, Electronics Instrument Support, Code 34 and Robert James, 11 September, 1995.

18. Private letter between R.C. Stiffler, Process Control and Measurement Technology Division, Aluminum Company of America and T.R. McNelley, Department of Mechanical Engineering, Naval Postgraduate School, 14 July, 1995.

19. Burley, C.E., *Eddy Current Standards in Nonferrous Metals*, "Proceedings of the Workshop on Eddy Current Nondestructive Testing," National Bureau of Standards, pp.39-43, 1981.

INITIAL DISTRIBUTION LIST

1. Defense Technical Information Center 2
   8725 John J. Kingman Rd., STE 0944
   Ft. Belvoir, Virginia 22060-6218

2. Dudley Knox Library..2
   Naval Postgraduate School
   411 Dyer Rd.
   Monterey, California 93943-5101

3. Chairman, Code ME 1
   Mechanical Engineering Department
   Naval Postgraduate School
   700 Dyer Rd., Rm 328
   Monterey, California 93943-5100

4. Dr. Terry R. McNelley, Code ME/MC 4
   Mechanical Engineering Department
   Naval Postgraduate School
   700 Dyer Rd., Rm. 328
   Monterey, California 93943-5100

5. Naval/Mechanical Engineering Curricular Office, Code 34 1
   Naval Postgraduate School
   700 Dyer Rd., Rm. 115
   Monterey, California 93943-5100

6. Dr. William Frazier, Code 6063 2
   Naval Air Warfare Center
   Warminster, Pennsylvania 18974

7. Mr. Dan Flaherty 1
   Flare Technology Inc.
   2869 Old Higgins Road
   Elk Grove Village, Illinois 60007

8. LT Robert B. James 2
   c/o Edwin and Betty James
   P.O. Box 262
   Chaptico, Maryland 20621